博士論文

A critical time window for dopamine actions on the structural plasticity of dendritic spines
(ドーパミンが側坐核スパイン形態可塑性に作用する鋭い時間枠)

柳下　祥

Table of contents

Summary

Animal behaviors are reinforced by subsequent rewards that follow the behaviors within a narrow time window. The reward is coded by the phasic activity of dopaminergic neurons in the ventral tegmental area, which densely innervates the medium spiny neurons (MSNs) in the nucleus accumbens, a key brain area for reinforcement learning in mammals. Glutamatergic synapses on dendritic spines of the MSNs also receive sensorimotor inputs that evoke action potentials (APs). These concurrent neuronal activities of synaptic inputs and APs can induce spike-timing-dependent plasticity (STDP). Here, I selectively stimulated dopaminergic and glutamatergic inputs on MSNs by optogenetic stimulation of dopaminergic fibers and two-photon uncaging of caged-glutamates paired with APs (STDP) in acute slices of mouse brain. I found that dopamine markedly potentiated spine enlargement, but this only occurred within a narrow time window (0.3–2 s), which is consistent with behavioral conditioning findings. FRET imaging of Ca^{2+}/calmodulin-dependent protein kinase II (CaMKII) and protein-kinase A (PKA) revealed that the sequence detection involved molecular signaling upstream of PKA activation: Sufficient generation of cAMP for PKA activation occurred only when spikes preceded dopamine to prime adenylyl-cyclase (AC1), otherwise cAMP was effectively removed by a potent phosphodiesterase activity

in thin distal dendrites of MSNs due to a large surface-to-volume ratio. Therefore, PKA was activated only within the specific timing for reinforcement, which then activated CaMKII through the dopamine- and cAMP-regulated phosphoprotein 32 kDa (DARPP-32). Thus, I have clarified the molecular basis of reinforcement plasticity which is operated at the level of single dendritic spines.

Introduction

Over a century ago, Thorndike and Pavlov realized that animal behaviors are reinforced only when rewarded shortly after a motor or sensory event (Thorndike, 1911; Pavlov, 1927). Following behavioral studies showed that natural reward effectively reinforced the preceding events when the delays were within 4 s (Bersh, 1951; Boice and Denny, 1965; Rescorla, 1988). A further study with electrical stimulation of reward circuit showed that the preceding motor events were strongly reinforced when reward circuit was stimulated within 1 s after the motor events (Black et al., 1985), suggesting that the neural mechanism could operate reward in a resolution as fine as 1 s.

The neocortex, hippocampus, and amygdala process the sensorimotor signals and send glutamatergic synaptic output to the striatum (Roitman et al., 2005), where connections can be modified by Hebbian learning mechanisms, such as spike-timing-dependent plasticity (STDP) (Dan and Poo, 2006). Animals learn to associate the sensorimotor signals with subsequent rewards by reinforcement of the neuronal circuits involving dopamine (Black et al., 1985; Schultz, 1998; Smith-Roe and Kelley, 2000). Behavioral studies have shown that the associative learning based on reward requires dopamine (Darvas et al., 2014) and its receptors (Smith-Roe and Kelley, 2000) in the nucleus accumbens (NAc) of the striatum. Because STDP in the striatal

neurons depended on dopamine (Shen et al., 2008), it has been postulated that the dopaminergic modulation of STDP underlies the associative learning (Surmeier et al., 2009; Surmeier et al., 2011).

However, the slow kinetics of dopamine-regulated kinase signaling contradicts the ability to detect the narrow time sequence of sensorimotor events and reward in the order of seconds. A recent study with Förster resonance energy transfer (FRET) imaging of protein-kinase A (PKA), the downstream signaling of dopamine, showed that in response to a brief dopamine stimulation (0.3 s), PKA was activated for more than one minute in striatal neuronal cells (Castro et al., 2013). So far, how the cellular signaling in the order of minutes detects the dopamine timing in the order of seconds remains elusive, and might be ascribed to neural network properties (Schultz, 1998; Nakano et al., 2013). Dendritic spine morphology is correlated with spine function (Matsuzaki et al., 2001), and dendritic spines enlarge during long-term potentiation in the cortices (Matsuzaki et al., 2004; Harvey et al., 2008; Tanaka et al., 2008). The principle neurons of the striatum, medium spiny neurons (MSNs), are also rich in the dendritic spines and express both glutamate receptors (Gracy and Pickel, 1996; Chen et al., 1998; Hara and Pickel, 2005) and dopamine receptors (Hara and Pickel, 2005). Thus I hypothesized that dendritic spines would detect the time sequence of glutamatergic and dopaminergic

inputs for the structural plasticity. However, it has been difficult to directly test the interaction of glutamate and dopamine signaling because the conventional electrical stimulation cannot separately stimulate glutamate and dopamine fibers which are intermingled in the striatal slice. Therefore, I sought to combine two optical stimulation methods: two-photon uncaging of caged-glutamate (Matsuzaki et al., 2001) and optogenetic stimulation of dopamine fibers that express channelrhodopsin-2 (Stuber et al., 2010; Tecuapetla et al., 2010). Two-photon uncaging by near-infrared laser allows to stimulate each single spines with high temporal resolution that is analogous to the endogenous glutamate release (Matsuzaki et al., 2001; Ellis-Davies et al., 2007). Optogenetic stimulation of axon terminals by wide-field irradiation of blue light causes transient dopamine release throughout the slice (Stuber et al., 2010), allowing temporal control of dopamine signaling and synchronized activation of several dopamine fibers. This can mimic the endogenous reward responses of dopamine where more than half of dopamine neurons fire in response to the reward (Cohen et al., 2012) that induces the elevation of tissue dopamine concentration in the striatum (Day et al., 2007).

Results showed that dopamine markedly promoted spine enlargement only during a narrow time window (0.3–2 s) following the glutamatergic inputs, consistent with behavioral conditioning (Black et al., 1985). The sequence detection was caused by

the rapid regulation of cAMP in thin distal dendrites, where protein-kinase A was activated only within the specific timing for reinforcement. Thus, I have clarified the molecular basis of reinforcement plasticity which is induced at the level of single dendritic spines.

Materials and Methods

Adeno-associated virus (AAV) preparation and animal surgery

I prepared an AAV vector that expressed mCherry driven by Preprotachykinin A (PPTA) promoter (PPTA-mCherry) to label the D1R-MSNs that constitute the direct pathway (Hikida et al., 2010). For the construction of pAAV-PPTA-mCherry and pAAV-PPTA-Cre, the PPTA promoter was cloned from the mouse as described previously (Hikida et al., 2010) and fused to mCherry or Cre in a AAV-expression vector. An AAV vector that expresses channelrhodopsin-2 (ChR2) in a Cre-dependent manner (EF1-DIO-hChR2(H134R)-mCherry) was a kind gift from K. Deisseroth.

AAV vectors were prepared and titered as described previously (Grieger et al., 2006). Briefly, plasmids for AAV vector, pHelper (Stratagene), and RepCap5 (Applied Viromics) were transfected to HEK293 cells (AAV293, Stratagene). After a 3-d incubation, cells were collected and purified by CsCl-gradient ultracentrifugation. CsCl was removed by dialysis. Titers for AAV were estimated by quantitative polymerase chain reaction (qPCR). An AAV vector for EF1-DIO-hChR2(H134R) was purchased from the U Penn Vector core.

For the labeling of dopamine neuron, I adopted the knock-in mouse line where an internal ribosome entry site (IRES) linked with Cre was introduced into the

downstream of the stop codon of the endogenous dopamine transporter (DAT) (Backman et al., 2006). This mouse line has been shown to express Cre in dopamine neurons with high specificity (Lammel et al., 2015; Stuber et al., 2015). A total of 1 μl AAV was injected bilaterally into nucleus accumbens (NAc; AP +1.3 mm, ML +/− 1.1 mm, DV + 4.3 mm) and ventral tegmental area (VTA; AP −3.4 mm, ML +/− 0.5 mm, DV +4.3 mm) of 3-week old DAT-IRES-Cre mice (B6.SJL-Slc6a3$^{tm1.1(cre)Bkmn}$/J, The Jackson Laboratory) with the infusion syringe pump (0.5 μl/min). Mice were allowed to recover for more than 2 weeks after the injection.

Acute slice preparation

Acute coronal slices of nucleus accumbens (280 μm) were obtained from 5- to 7-week-old mice that were injected with AAV. Mice were anesthetized by ketamine and xylazine; perfused transcardially by ice-cold solution containing 220 mM sucrose, 3 mM KCl, 8 mM $MgCl_2$, 1.25 mM NaH_2PO_4, 26 mM $NaHCO_3$, and 25 mM glucose; and then quickly decapitated to prepare slices with a VT1200 microtome (Leica). The slices were incubated at 34°C for 30 min and then at room temperature in artificial cerebrospinal fluid (ACSF; 125 mM NaCl, 2.5 mM KCl, 1 mM $CaCl_2$, 2 mM $MgCl_2$, 1.25 mM NaH_2PO_4, 26 mM $NaHCO_3$, and 20 mM glucose), which was bubbled with

95% O_2 and 5% CO_2. The slices were transferred to a recording chamber and superfused with the same ACSF above except for 2 mM $CaCl_2$, 1 mM $MgCl_2$, and 200 μM Trolox (Sigma). All physiological experiments were performed at 30–32°C.

In experiments with D-AP5 (50 μM, Tocris), KN62 (3 μM, Wako), SCH23390 (3 μM, Wako), sulpiride (10 μM, Wako), KT5720 (2 μM, Sigma-Aldrich), calyculin A (50 nM, Wako), tautomycetin (4 nM, Tocris), and papaverine (Nishi et al., 2008) (10 μM, Wako), slices were superfused for at least 30 min with each inhibitor before glutamate uncaging. In experiments with anisomycin (5 μM, Sigma-Aldrich), slices were incubated with anisomycin for at least 1 h before glutamate uncaging. The experimental protocol was approved by the Animal Experimental Committee of the Faculty of Medicine, the University of Tokyo.

Two-photon imaging

Two-photon imaging of dendritic spines was performed with an upright microscope (BX61WI, Olympus) equipped with an FV1000 laser-scanning microscope system (FV1000, Olympus) and a water-immersion objective lens (LUMPlanFI/IR, 60×, numerical aperture 1.0). The system included two mode-locked, femtosecond-pulse Ti:sapphire lasers (MaiTai from Spectra Physics). One was set at a wavelength of 720 nm

for the uncaging of glutamate and the other was set at 980 nm for Alexa 488 and Fluo-4FF or 940 nm for Förster resonance energy transfer (FRET) imaging. Each of the lasers was connected to the microscope via an independent scan head and gated with an acoustico-optic modulator for two-photon uncaging of caged-glutamate and imaging. For ChR2 stimulation, optical fiber (500 μm core, BFH22-550, Thorlab) connected to a blue diode laser (457 nm, 15−20 mW, 5 ms, Lucir) was placed near the imaging site (~300 μm).

Dendrites containing spines within 100 μm from the soma (typically the second to fourth branches) and 20−35 μm in depth were used for the imaging and uncaging experiments unless otherwise noted. Three-dimensional reconstructions of dendritic morphology were generated by the summation of fluorescent values separated by 0.5 μm. The fluorescence of dendrites continued to increase gradually even 20 min after whole-cell perfusion and was corrected by the entire fluorescence of an imaging area where dendritic fluorescent signals were predominant. The spine-head volumes were estimated from the total fluorescence intensity. Neighboring spines were defined as spines within 3 μm of the stimulated spines.

Electrophysiology

For whole-cell recordings, the patch-clamp electrode (open-tip resistance, 5−8 MΩ) was filled with a solution containing 120 mM potassium gluconate, 20 mM KCl, 10 mM disodium phosphocreatine, 50 μM Alexa 488 (Life Technologies), 4 mM ATP (magnesium salt), 0.3 mM GTP (sodium salt), 10 mM HEPES, and 5 μM β-actin (human platelets; Cytoskeleton). The pH was adjusted to 7.25 with KOH, and the osmolarity was adjusted to 275−280 mOsm/l with sucrose. In experiments with protein-kinase A inhibitor (PKI , 10 μM PKI [5−24] , Promega), autocamtide-2-related inhibitory peptide (AIP; 5 μM, Sigma-Aldrich), NB001 (50 μM, Sigma-Aldrich)(Wang et al., 2011; Corder et al., 2013), dopamine- and cAMP-regulated phosphoprotein 32 kDa (DARPP-32) inhibitory peptide (Kwon et al., 1997) (DARPP-32 [1−22], 100 μM, BEX, custom peptide synthesis), DARPP-32 control peptide (DARPP-32 [8−22], 100 μM, BEX, custom peptide synthesis), inhibitors were included in the recording pipette and were allowed to perfuse at least 20 min after beginning whole-cell recording. The cells were voltage-clamped at −70 mV except during stimulation. Cells with a resting potential >−60 mV during the stimulating period were discarded before plasticity induction.

I locally puffed CDNI (4-Carboxymethoxy-5,7-Dinitroindolinyl)-glutamate (Ellis-Davies et al., 2007) (4 mM) from a glass pipette positioned close to the selected

dendrite. For experiments with continuous application of dopamine, dopamine (100 μM) (Matsuda et al., 2006) was also included in the puff pipette. The laser power was set 5−6 mW with activation time of 0.6 ms to evoke currents through AMPA (α-amino-3-hydroxy-5-methyl-4-isoxazolepropionic acid)-sensitive glutamate receptors with an amplitude of approximately 5–20 pA. This stimulation also evoked excitatory-postsynaptic potentials (EPSPs) similar to miniature excitatory-postsynaptic potentials (mEPSPs, Fig. 1G). The signals were evoked three to five times at each time point, low-pass filtered at 2 kHz, sampled at 10 kHz, and then averaged. For each experiment, ChR2 expression at the presynaptic fibers was confirmed by evoking an excitatory postsynaptic current (EPSC) with blue laser stimulation, which co-releases glutamate from the DA fiber (Tecuapetla et al., 2010).

Structural plasticity was induced by the following spike-timing-dependent plasticity (STDP) protocol (Shen et al., 2008) consisted of 15 trains of 10 bursts repeated at 0.1 Hz. Each burst was composed of three back-propagating APs (bAPs, 100 Hz) preceded by a single 2pEPSP (Δt = +10 ms) stimulated by two-photon uncaging of CDNI-glutamate at a wavelength of 720 nm. For each experiment, three to four spines were stimulated. To mimic the up-state, which may facilitate plasticity induction, a small depolarizing holding current (~120 pA) was applied to maintain voltage near −55

mV from 100 ms before the onset until the end of STDP stimulation (in total, 1.1 s). APs were induced by injection of a depolarizing current of 0.6−1 nA for 2 ms. The STDP protocol was combined with optical stimulation (457 nm, 5 ms, 30 Hz, 10 times) of dopaminergic fibers expressing ChR2 (DA_{opto}) at various time points relative to the onset of STDP stimulation.

To examine long-term potentiation of EPSCs (Fig. 5), the same STDP protocol was used, except that glutamate uncaging was replaced with electrical stimulation of presynaptic fibers with theta-glass electrode (2 ms, 12−50 μA) which was placed 80−150 μm from the patch pipette. Test stimuli were applied every 15 s. Data were excluded when the series resistance changed more than 20 % over the time course of the experiment.

Amperometry

I confirmed that the optogenetically induced signal occurred at the peak current at 0.6 mV, which is consistent with the dopamine-induced oxidation current, using fast-scan cyclic voltammetry (from −0.5 V to 1.2 V at rate of 400V/s, scanning rate 10 Hz). The temporal characteristic of dopamine release in response to optogenetic stimulation was evaluated by constant-potential amperometry (Tritsch et al., 2012),

which has high temporal resolution. Carbon-fiber microelectrodes with a small tip (Carbostar-1, 5−8 μm diameter, ~20 μm length, Kation Scientific) were placed 40−60 μm below the surface of the nucleus accumbens slice. The electrode potential was held at a constant voltage of 600 mV versus Ag/AgCl by ChemClamp (Dagan). Electrodes were calibrated with 0, 1, and 5 μM dopamine hydrochloride (Wako) in ACSF.

Ca^{2+} imaging

For Ca^{2+} measurements, the pipette solution contained Ca^{2+} sensitive 500 μM Fluo-4FF (Life Technologies) and non-sensitive 50 μM Alexa 594 (Life Technologies) fluorescent dye instead of Alexa 488. Images were acquired at 10 Hz. Fluorescence intensities were measured at 485−555 nm (*G*) and 598−672 nm (*R*) for Fluo-4FF and Alexa 594, respectively. I obtained the ratios $\Delta G/G_0 = (G(t)-G_0)/G_0$, where $G(t)$ is the fluorescence intensity at time *t*, and G_0 is the average intensity before stimulation.

Förster resonance energy transfer (FRET) imaging

AAV expression vectors carrying FRET probes were constructed by replacing CaMKII(0.3) promoter with EF1 and hChR2(H134R)-mCherry with Camuiα-CR or AKAR2-CR (Lam et al., 2012), which were kind gift from Dr. Lin. For CaMKII FRET

imaging, D1R-MSNs were sparsely labelled (Xu et al., 2012) by co-injection of diluted PPTA-Cre and high titer CaMKII(0.3)-DIO-Camuiα-CR AAV vectors to nucleus accumbens. An AAV vector for EF1-DIO-hChR2(H134R)-mCherry was also injected into the ventral tegmental area. For PKA FRET imaging, an AAV vector expressing AKAR2-CR was injected instead of Camuiα-CR. Images were acquired at 2 Hz for distal dendrite and spine imaging with a single plane and 0.5 Hz with three to five z-stacks for soma and adjacent dendrite imaging. Fluorescence intensities were measured at 485−555 nm (*G*) and 598−672 nm (*R*) for Clover and mRuby2, respectively. Images were down sampled to 0.16 Hz for distal dendrites or 0.08 Hz for soma to improve the signal-to-noise ratio, and XY image drift was registered to the first image. For each region-of-interest (spine, dendrite, or soma), I obtained the ratios $\Delta r/r_0 = (r(t)-r_0)/r_0$, where $r(t)$ is the ratio of fluorescence intensity in G and R at time *t*, and r_0 is the average ratio before stimulation. Specifically, the $r(t)$ for Camuiα-CR activation was calculated as G divided by R, and $r(t)$ for AKAR2-CR activation was calculated as R divided by G, so that $\Delta r/r_0$ indicates the increase in the activity of each kinase that the FRET probe monitors. Channel bleeding was not corrected. For image display, Gaussian convolution with a standard deviation (SD) of 10 pixels, which corresponded to 0.55 μm for images of distal dendrites and 1.1 μm for images of soma,

was applied for each G and R. The ratio images were created by calculating the ratio for each pixel, and then, the images were normalized to the images before stimulation and the relative ratio increases were pseudocolor coded.

Immunohistochemistry

The specificity of gene expression by AAV was assessed by immunohistochemistry. Mice injected with AAV were allowed to incubate more than 2 weeks and then were anesthetized (ketamine, xylazine) and perfused transcardially with 4% paraformaldehyde in phosphate-buffered saline (PBS). Slices (60-μm thick) containing the nucleus accumbens or ventral tegmental area were prepared using a vibratome. For nucleus accumbens slices, antigen retrieval was made by 10 mM sodium citrate for 30 min at 80°C. The slices were incubated with either anti-substance P (SA1270, Enzo Life Sciences, 1:400), anti-Met-enkephalin (EA1150, Enzo Life Sciences, 1:400) or anti tyrosine hydroxylase antibody (AB152, Millipore, 1:400−800) in PBS containing 5% normal goat serum, 0.2% Triton X, and 0.1% NaN_3 for 48 h at 4°C. After washing with PBS, slices were incubated with Anti-rabbit IgG antibody conjugated with Alexa488 (1:400) for 2 h at room temperature, then reacted with TO-PRO-3 (Life Technologies) for nuclear staining. The slices were mounted with

anti-fading reagents (Vectashield, Vector Laboratories) and Z-stack images were acquired with confocal microscopy (BX-61, Olympus). The images were analyzed using ImageJ. For each of neuron expressing mCherry either driven by the PPTA promoter or fused with ChR2, the immunofluorescent signal was regarded as positive for the cell if the Alexa 488 signal continuously covered more than half of the soma at the Z level of peak TO-PRO-3 fluorescence.

Data analysis

Two-photon images were analyzed with ImageJ (National Institutes of Health) and a custom-made program running on Matlab (Mathworks Inc.). The electrophysiological data analyses and all statistical analyses were performed with Excel (Microsoft) and Excel Statistics (SSRI). For all spine volume analyses, volume changes at 40 min and 50 min after plasticity induction were averaged and used in the statistical analyses. For calcium imaging, the peak values (1 s after stimulation onset) were used in the statistical analyses. For FRET imaging, the averaged values of the time points spanning 12 s around the peak were included in the statistical analyses. Data are presented as mean ± s.e.m., and differences were analyzed by Mann-Whitney U tests or Kruskal–Wallis

one-way analysis of variance (ANOVA) followed by Steel's post hoc test. $P < 0.05$ was considered statistically significant.

Results

I investigated dopamine actions on glutamatergic synapses on medium spiny neurons (MSNs) using optogenetics and two-photon uncaging. For optogenetic stimulation of dopaminergic fibers, a Cre-dependent adeno-associated virus (AAV) vector expressing channelrhodopsin-2 (ChR2) was injected into the ventral tegmental area (VTA) of DAT-Cre mice expressing Cre specific to dopaminergic neurons (Fig. 1A). Immunohistochemical analysis of VTA slice from AAV injected mice showed that 94 % of neurons expressing ChR2 fused with mCherry were stained with anti-tyrosine hydroxylase antibody, a maker for dopamine neurons. The direct pathway constituting MSNs, which express dopamine 1 receptors (D1Rs) and substance P peptide (Gerfen et al., 1990), were labeled by an AAV vector with the promoter for Preprotachykinin A (PPTA), a precursor protein for substance P (Fig. 1A) (Hikida et al., 2010). Immunohistochemical analysis of nucleus accumbens (NAc) slice showed that 89% of neurons expressing mCherry driven by PPTA promoter were positive for anti-substance-P antibody while 14% neurons expressing mCherry were positive for anti-enkephalin antibody, a maker for dopamine 2 receptor expressing MSN (Fig. 1C).

In acute coronal slices, including the nucleus accumbens core, whole-cell recordings were obtained from the identified D1R-MSNs. Dendritic spines were

visualized by two-photon microscopy (980 nm) detecting fluorescence of Alexa488 loaded through a recording pipette (Fig. 1D, E). Stimulation of a single spine by two-photon uncaging (720 nm) of CDNI (4-Carboxymethoxy-5,7-Dinitroindolinyl)-Glu (Fig. 1F) induced two-photon excitatory postsynaptic potentials (2pEPSPs) with amplitudes similar to miniature EPSPs (mEPSPs; Fig. 1G). The amplitudes of 2pEPSCs positively correlated with spine volumes, as they did with pyramidal neurons (Fig. 1H) (Matsuzaki et al., 2001). A single pulse of blue laser stimulation of ChR2-expressing dopaminergic fibers induced a transient increase in the tissue dopamine concentration (Fig. 1F).

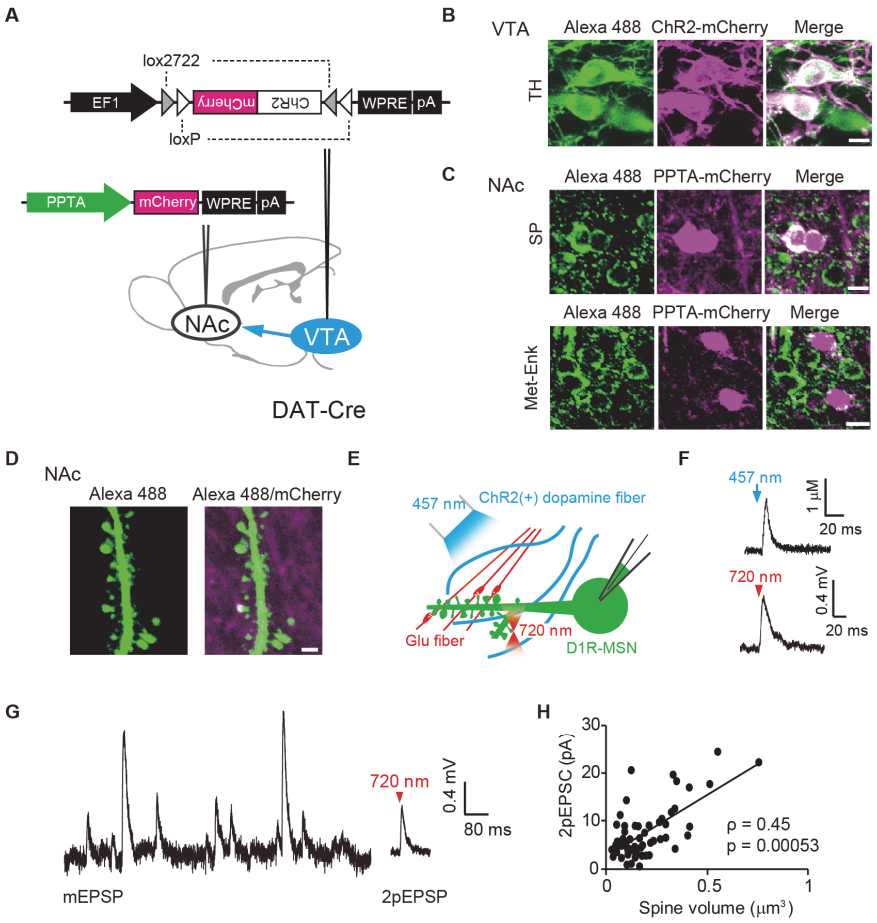

Fig. 1. Immunohistochemistry and two-photon glutamate uncaging.

(**A**) Injection of AAV vectors for ChR2 and the D1R-MSN marker (PPTA-mCherry) in 3-week-old DAT-Cre mice. (**B**) Immunohistochemical analysis of VTA slices expressing mCherry fused with hChR2 with anti-tyrosine hydroxylase antibody with Alexa 488. Among 195 neurons expressing mCherry, 184 (94%) neurons were positive for tyrosine hydroxylase. Scale bar, 10 μm. (**C**) Immunohistochemical analysis of NAc slices expressing mCherry under the control of a PPTA promoter with anti-substance-P (left) or anti-met-enkephalin antibody labeled by secondary antibody conjugated with Alexa 488 (right). The fluorescence signal of mCherry overlapped with the D1R-MSN marker substance P but not with the D2R-MSN marker met-enkephalin (Gerfen et al., 1990). Among 95 neurons expressing mCherry, 85 (89%) neurons were positive for substance-P. In contrast, among 76 neurons expressing mCherry, 11 (14%) neurons were positive for met-enkephalin. SP, anti-substance P antibody, Met-Enk,

anti-met-enkephalin antibody. Scale bar, 10 μm. (**D**) Visualization of dendritic spines from a D1R-MSN with fluorescence emitted by Alexa 488 loaded through the recording pipette, and the overlay image on the ChR2-mCherry-expressing dopaminergic fibers and PPTA-mCherry-expressing neurites of MSNs. Scale bar, 2 μm. (**E**) Selective stimulation of dopaminergic and glutamatergic inputs by blue laser field irradiation to ChR2 and two-photon uncaging of caged-glutamate at a single spine, respectively, in acute slices of NAc obtained from 5–7-week-old mice. (**F**) An amperometric measurement of dopamine (upper panel) by carbon-fiber electrode and whole-cell recording of glutamate-induced current (lower panel, 2pEPSP) in identified D1R-MSNs. (**G**) Current clamp recording from an identified D1R-MSN showing an mEPSP (left) and two-photon uncaging of caged glutamate-induced EPSP (2pEPSP). The 2pEPSP is the average of five recordings. (**H**) Spine structure-functional relationship in MSNs (56 spines). Spine volumes and the peak 2pEPSC amplitudes for individual spines were plotted. The Spearman's correlation coefficient was 0.45 with $P = 0.00053$.

The spike-timing-dependent plasticity (STDP) protocol of repetitive uncaging of glutamate paired with APs (Fig. 2A; Glu + AP)(Shen et al., 2008) induced robust spine enlargement that was selective for the stimulated spine (Fig. 2B, C) when dopamine (100 μM) was puff applied, whereas only a weak enlargement occurred in the absence of dopamine (Fig. 2D, E). This result is consistent with previous findings showing the dependence of the plasticity on dopamine in the striatal neurons (Reynolds et al., 2001; Shen et al., 2008).

Then I tested the actions of a physiologically-relevant phasic release of dopamine (30 Hz, 10 times) induced by the optogenetic stimulation of dopaminergic fibers (DA_{opto}), and found that DA_{opto} just after STDP stimulation (DA_{opto} delay = 1 s, Fig. 3A) induced robust spine enlargement (Fig. 3B, C). Then the actions of DA_{opto} were examined with various timings (Fig. 3D-J) that consisted of stimulation of dopaminergic fibers 1 s before (DA_{opto} delay = −1 s, Fig. 3D), simultaneously (DA_{opto} delay = 0 s, Fig. 3E), 0.3 s after (DA_{opto} delay = 0.3 s) STDP (Fig. 3F), 0.6 s after (DA_{opto} delay = 0.6 s) STDP (Fig. 3G), 2 s after (DA_{opto} delay = 2 s) STDP (Fig. 3H), and 5 s after (DA_{opto} delay = 5 s) STDP (Fig. 3I). The change in the spine volume was plotted versus the DA_{opto} delay, revealing that DA_{opto} timing was critical to enhance plasticity, with maximal effects for a delay of 0.6

seconds (Fig. 3K), and decayed in a few seconds, consistent with behavioral study results (Black et al., 1985; Rescorla, 1988).

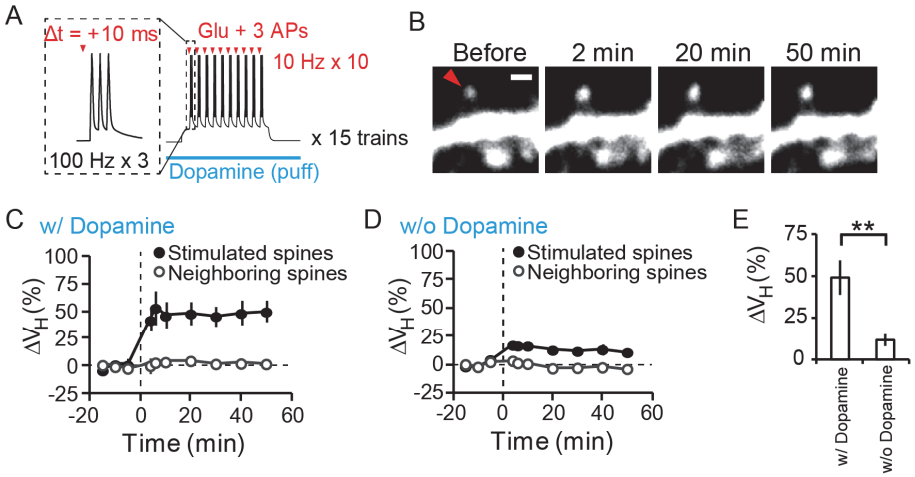

Fig. 2. Spike-timing-dependent plasticity (STDP) protocol induced structural plasticity with or without dopamine puff application.

(**A**) An STDP protocol with dopamine puff application. (**B**) Images of the dendritic spine (red arrowhead) that received STDP stimulation in the presence of dopamine (100 μM). (**C**, **D**) Time courses of spine enlargement in the presence (C, 13 spines, 4 dendrites) and absence of dopamine (D, 58 spines, 14 dendrites). (**E**) Amplitudes of spine enlargements with or without dopamine. ***P* = 0.0041 by Mann-Whitney U test.

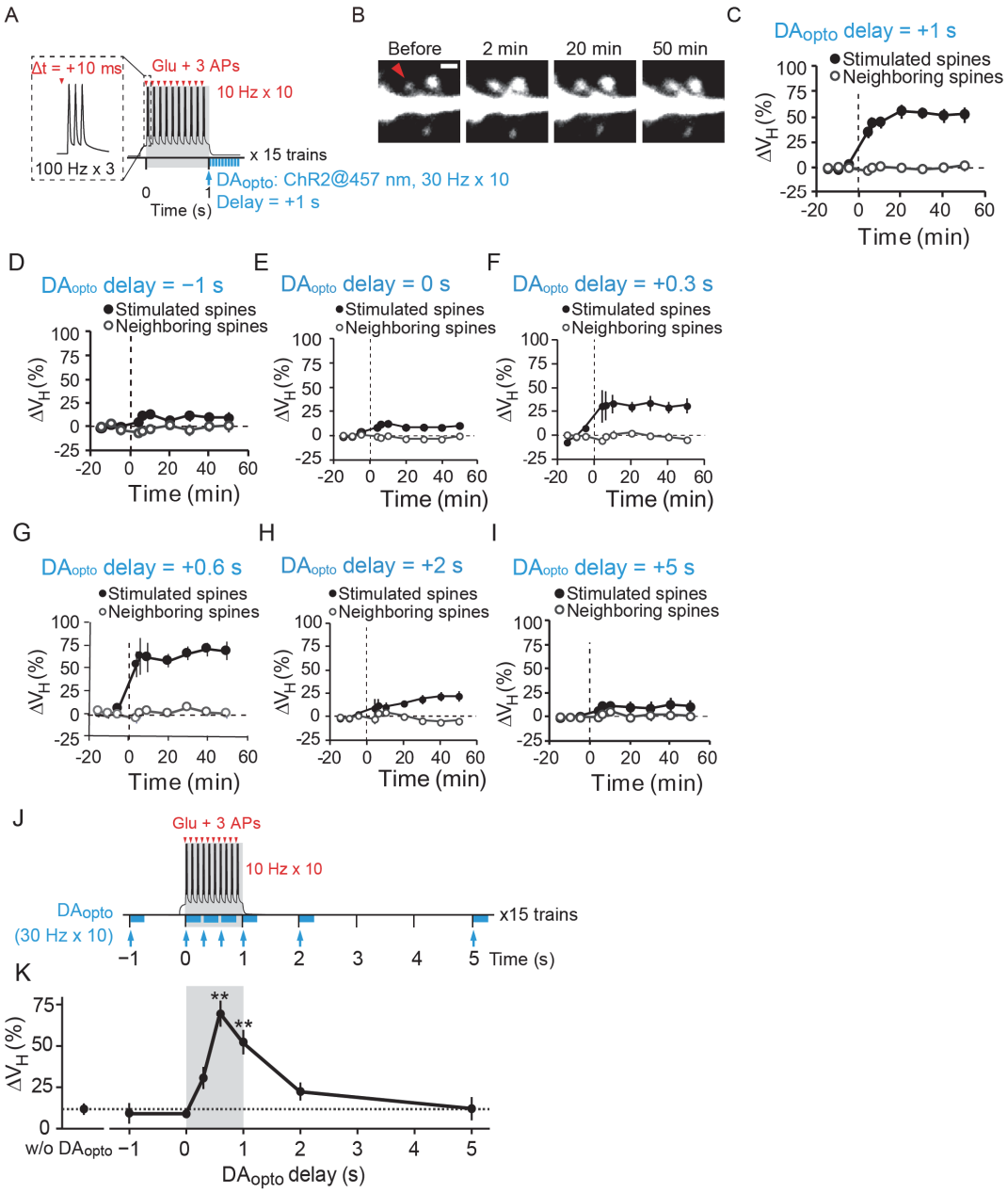

Fig. 3. STDP protocol with DA_{opto} at various delays.

(**A**) STDP with repetitive activation of dopaminergic fibers containing ChR2 (blue lines) at 30 Hz, 10 times (DA_{opto}) with a delay of 1 s. (**B**) Images of the dendritic spine (arrowhead) that received STDP + DA_{opto} with a delay of 1 s. (**C-I**) Time courses of spine enlargement induced by STDP + DA_{opto} at 1 s (C, 48 spines, 14 dendrites), –1 s (D, 20 spines, 5 dendrites), 0 s (E, 42 spines, 10 dendrites), 0.3 s (F, 20 spines, 5 dendrites),

0.6 s (24 spines, 7 dendrites), 2 s (H, 28 spines, 7 dendrites). and 5 s (I, 28 spines, 7 dendrites) after STDP onset. (**J**) STDP with various delays of DA_{opto} application. (**K**) Increases in spine volumes by STDP + DA_{opto} plotted versus DA_{opto} delay. $P = 4.2 \times 10^{-6}$ with Kruskal–Wallis and $^{**}P = 0.0018$ (0.6 s) and 0.0027 (1 s) by Steel test in comparison with STDP in the absence of DA_{opto}. Data are presented as mean ± s.e.m. Scale bars indicate 1 μm.

In hippocampal neurons, the spine enlargement was accompanied by an increase in the 2pEPSC (Matsuzaki et al., 2004). Thus I recorded 2pEPSC from spines stimulated with STDP in the presence or absence of DA_{opto} (Fig. 4A–F). In STDP with DA_{opto} condition, the stimulated spines showed increases in 2pEPSC and spine volume while neighboring spines did not (Fig. 4A, D). In contrast, no increase in 2pEPSC or spine volume was observed in the spines stimulated with STDP in the absence of DA_{opto} (Fig. 4B, E). There were significant effects of DA_{opto} on 2pEPSC and spine enlargement (Fig. 4C, F). Therefore, the spine enlargement was accompanied by the 2pEPSC increase in D1R-MSNs, suggesting that the structural plasticity is the basis for long-term potentiation (LTP) in D1R-MSNs, similar to hippocampal neurons.

Next I tested whether a similar DA_{opto} timing was observed when plasticity was induced by STDP protocol with electrical stimulation of presynaptic fibers instead of uncaging of caged-glutamate (Fig. 5A). LTP was successfully induced by STDP with electrical stimulation (eSTDP) when DA_{opto} was applied with a delay of 0.6 s (Fig. 5B, C). However, LTP was not observed in eSTDP in the absence of DA_{opto}, or in the presence of DA_{opto} with delays of 0 s and 2 s (Fig. 5C). In summary, the DA_{opto} timing for LTP induced by electrical stimulation was similar to the timing for spine enlargement induced by uncaging of caged-glutamate (Fig. 5D).

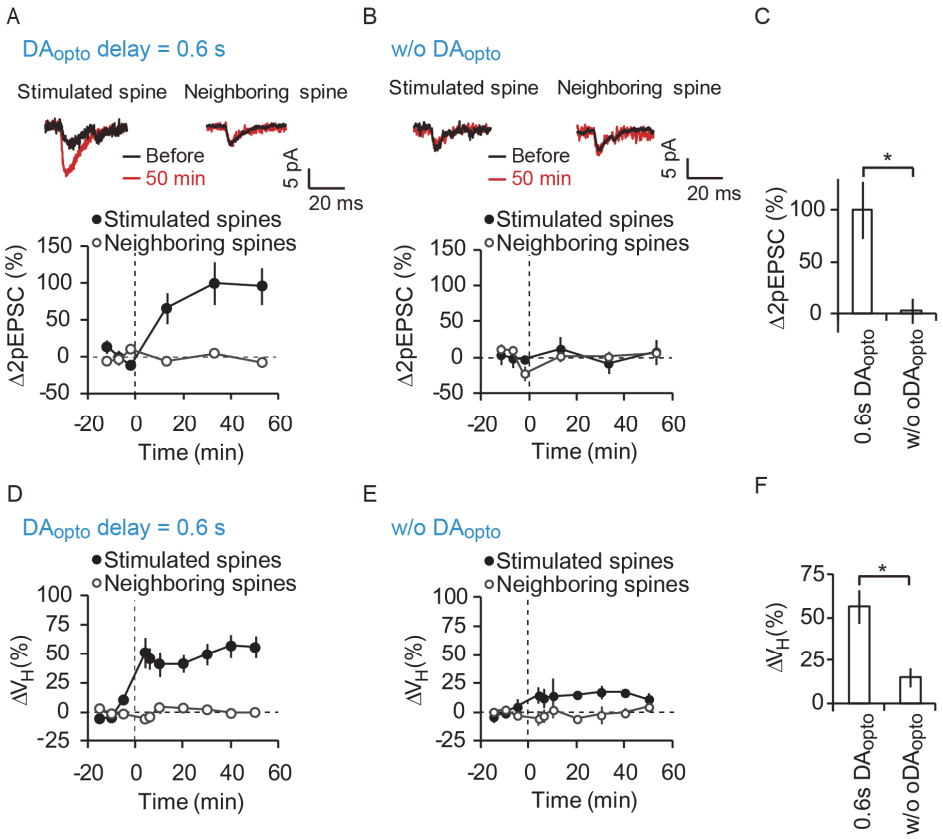

Fig. 4. Increases in 2pEPSCs followed spine enlargement.

(**A, B, D, E**) Time courses of the 2pEPSC amplitudes (A, 10 spines, 6 dendrites; B, 7 spines, 4 dendrites) and spine volume (D, E) in response to STDP + DA_{opto} with delays of 0.6 s (A, D) or without DA_{opto} (B, E). The data for 2pEPSC and spine volume were derived from the same spines. Insets in (A, B) show 2pEPSC for stimulated and neighboring spines before (black) and after the STDP protocol (red). (**C**, **F**), Average changes in 2pEPSCs (C) and spine volumes (F). Data are presented as mean ± s.e.m. * $P = 0.033$ (C) and 0.033 (F) with Mann-Whitney U test.

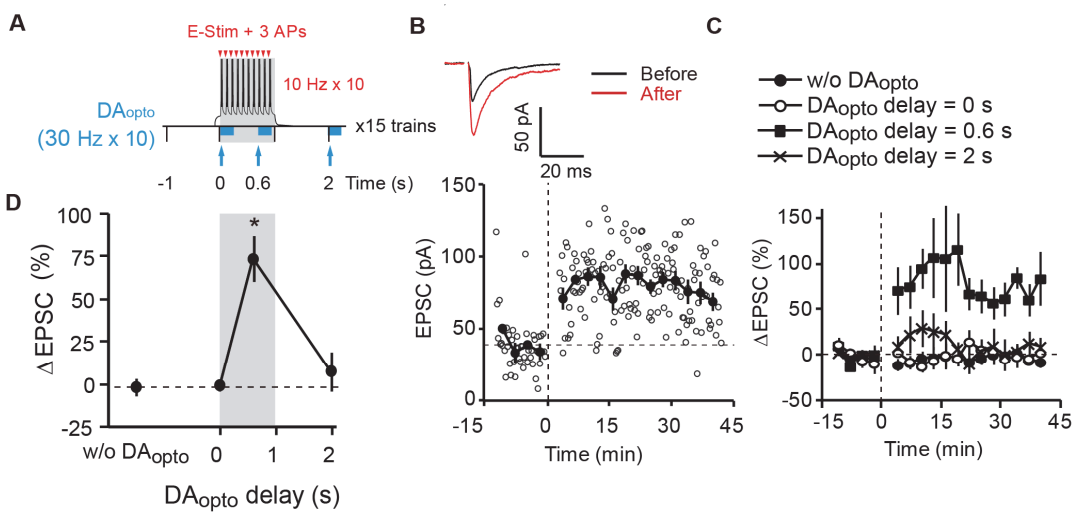

Fig. 5. DA_{opto} timing dependence of long-term potentiation of EPSCs (LTP).
(**A**) The STDP protocol with electrical stimulation of presynaptic fibers (eSTDP). The protocol was the same as Fig. 1I, except that glutamate uncaging was replaced with electrical stimulation. DA_{opto} was applied at three different time points from the onset of eSTDP. (**B**) An example of LTP induced by eSTDP + DA_{opto} with a delay of 0.6 s. Open circles represent the amplitudes of EPSCs evoked by test stimuli applied every 15 s, while filled circles the average amplitudes of 12 successive EPSCs. The inset shows the averaged EPSCs before (black) and 28 to 40 min after induction (red) of LTP. (**C**) The averaged time courses of EPSC amplitudes in response to eSTDP in the absence of DA_{opto} (filled circles, 7 cells) or in the presence of DA_{opto} with delays of 0 s (open circles, 5 cells), 0.6 s (squares, 5 cells), and 2 s (crosses, 6 cells). (**D**) The amplitudes of LTP plotted vs. DA_{opto} delay. $P = 0.0086$ with Kruskal–Wallis and $*P = 0.013$ (0.6 s) by Steel test vs. eSTDP without DA_{opto}. Data are presented as mean ± s.e.m.

Pharmacological studies were conducted to clarify the molecules involved in the structural plasticity of D1R-MSN (Fig 6A–D). Previous studies showed that structural plasticity in the hippocampus depended on *N*-methyl-D-aspartate receptors (NMDARs), Ca^{2+}/calmodulin-dependent protein kinase II (CaMKII), and protein synthesis (Matsuzaki et al., 2004; Harvey et al., 2008; Tanaka et al., 2008). Consistent with these reports, the spine enlargement in D1R-MSN was abolished by NMDAR antagonist (50 μM AP5), CaMKII inhibitor (3 μM KN62), CaMKII inhibitory peptide (5 μM autocamtide 2-related inhibitory peptide, AIP, in the pipette) and protein synthesis inhibitor (5 μM anisomycin) (Fig. 6A, C, D), suggesting that the molecular mechanisms for spine enlargement of D1R-MSN are similar to those of hippocampal neurons. In D1R-MSNs, protein-kinase A (PKA) is activated by dopamine through D1R, Gs and cAMP pathway and modulates electrically-induced plasticity (Calabresi et al., 2000; Shen et al., 2008). Therefore, I examined whether this pathway was also involved in the structural plasticity. As a result, spine enlargement was inhibited by D1R antagonist (3 μM SCH23390) and PKA inhibitory peptide (10 μM PKI in the pipette), and PKA inhibitor (2 μM KT5720) but not by D2R antagonist (10 μM sulpride) (Fig. 6B, C, D). These results indicate that DA_{opto} enhances plasticity through the activation of D1R/Gs/cAMP/PKA pathway.

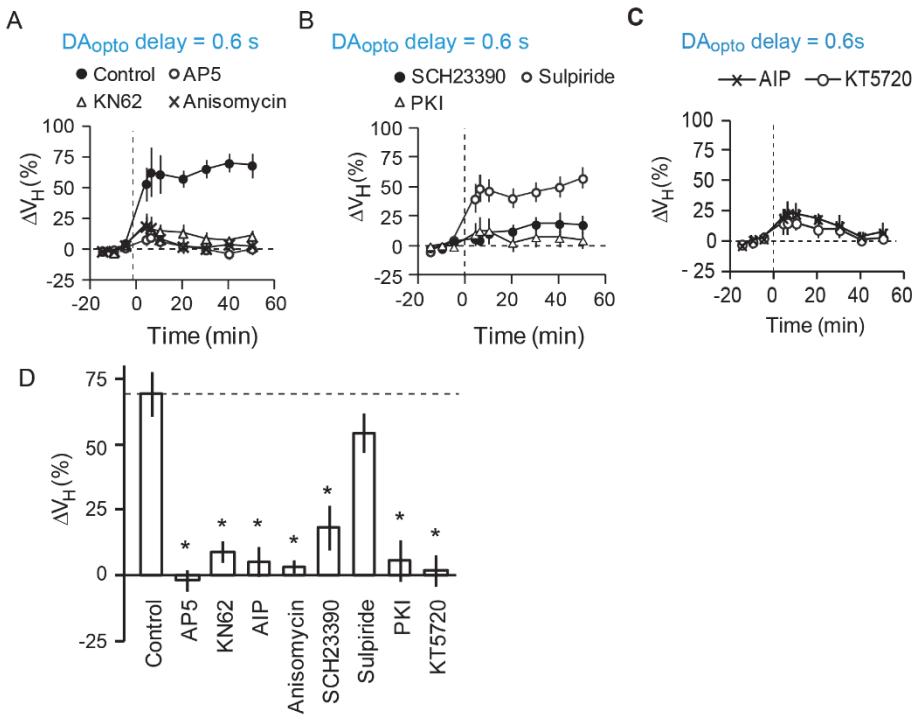

Fig. 6. Pharmacology of spine enlargement induced by STDP plus DA_{opto} with a 0.6-s delay.

(**A**) Time courses of spine enlargement induced by STDP + DA_{opto} with a 0.6-s delay in the absence (Control, the same as Fig. 3G) and presence of NMDAR antagonist (50 μM D-AP5, 22 spines, 6 dendrites), CaMKII inhibitor (3 μM KN62, 23 spines, 6 dendrites), or protein synthesis inhibitor (5 μM anisomycin, 25 spines, 6 dendrites). (**B**) Time courses of spine enlargement in the presence of D1R antagonist (3 μM SCH23390, 23 spines, 6 dendrites), D2R antagonist (10 μM sulpiride, 22 spines, 6 dendrites), or PKA inhibitor (10 μM PKI, in the pipette, 24 spines, 6 dendrites). (**C**) Time courses of spine enlargement induced by STDP + DAopto with a 0.6 s delay in the presence of CaMKII inhibitor (5 μM AIP in the pipette, 20 spines, 5 dendrites) or PKA inhibitor (2 μM KT5720, 20 spines, 5 dendrites). (**D**) Averaged volume changes in the absence and presence of the compounds. Data are presented as mean ± s.e.m. $P = 5.0 \times 10^{-5}$ with Kruskal–Wallis and *$P = 0.019$ (AP5), 0.019 (KN62), 0.031 (AIP), 0.019 (anisomycin), 0.029 (SCH23390), 0.019 (PKI), and 0.031 (KT5720) with Steel test.

Because previous studies suggested the interaction between D1R and NMDAR modulated the Ca^{2+} influx through NMDAR (Cepeda and Levine, 2006), I tested whether changes in Ca^{2+} signaling account for DA_{opto} timing for the plasticity. I recorded increases in cytosolic Ca^{2+} concentrations ($[Ca^{2+}]_i$) in spines using a low-affinity calcium indicator Fluo-4FF (K_{Ca} = 10 μM) to avoid saturation. The $[Ca^{2+}]_i$ increases gradually built up and quickly waned after cessation of the single train of STDP stimulation (Fig. 7A). Then, DA_{opto} was applied to STDP stimulation at delays of −1 s (Fig. 7B), 0 s (Fig. 7C), 0.6 s (Fig. 7D), and 2 s (Fig. 7E). The peak values were plotted against DA_{opto} delay (Fig. 7F, G), showing that DA_{opto} did not affect Ca^{2+} transients. This result indicates that Ca^{2+} signaling modulation did not play a major role.

Then, I examined whether CaMKII activation, a key molecule regulating spine enlargement (Lee et al., 2009), was related to DA_{opto} timing by employing the Förster resonance energy transfer (FRET) indicator of CaMKII, Camuiα-CR (Takao et al., 2005; Lee et al., 2009; Lam et al., 2012), which was virally transfected into D1R-MSNs. CaMKII activation of the spine stimulated by a single train of STDP protocol was weak in the absence of DA_{opto} (Fig. 8A), but was greatly potentiated by DA_{opto} with a delay of 0.6 s (Fig. 8B). This enhancement was specific to the stimulated spine (Fig. 8C). I further recorded CaMKII activation by STDP with DA_{opto} delays of −1 s (Fig. 8D), 0 s (Fig. 8E),

and 2 s (Fig. 8F). The peak values were plotted against DA_{opto} delay, showing a similar timing to spine enlargement for the enhancement (Fig. 8G). These results suggest that DA_{opto} gated CaMKII activity for the plasticity in DA_{opto} timing dependent manner.

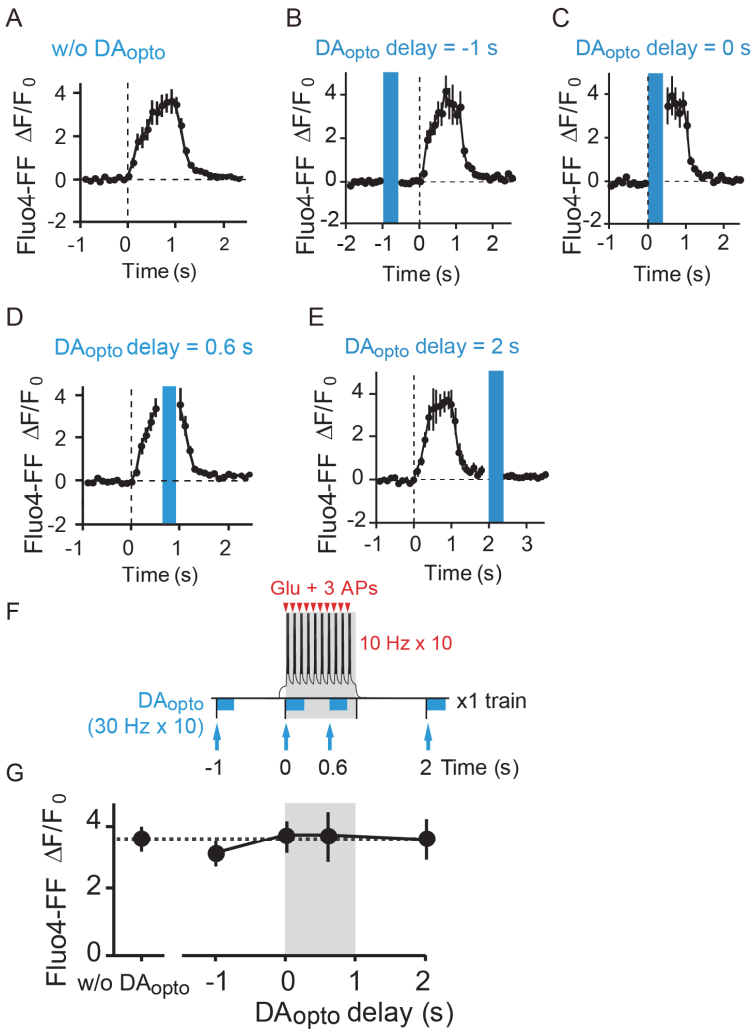

Fig. 7. DA_{opto} effects on STDP stimulation-induced increases in $[Ca^{2+}]_i$.

(**A–E**) Increases in Fluo4-FF fluorescence, representing $[Ca^{2+}]_i$ increases, within single spines in response to a train of STDP stimulation in the absence (A, 20 spines, 15 dendrites) and presence of DA_{opto} with delays of –1 s (B, 11 spines, 5 dendrites), 0 s (C, 9 spines, 3 dendrites), 0.6-s (D, 15 spines, 8 dendrites) and 2 s (E, 11 spines, 5 dendrites). Blue laser irradiation during DA_{opto} is blanked by the blue bar. (**F**) STDP and DA_{opto} protocols for Ca^{2+} and CaMKII imaging. Unlike plasticity induction (Fig. 3K), only one train was applied. (**G**) No effect of DA_{opto} on the peak values of $[Ca^{2+}]_i$. P = 0.91 with Kruskal–Wallis test.

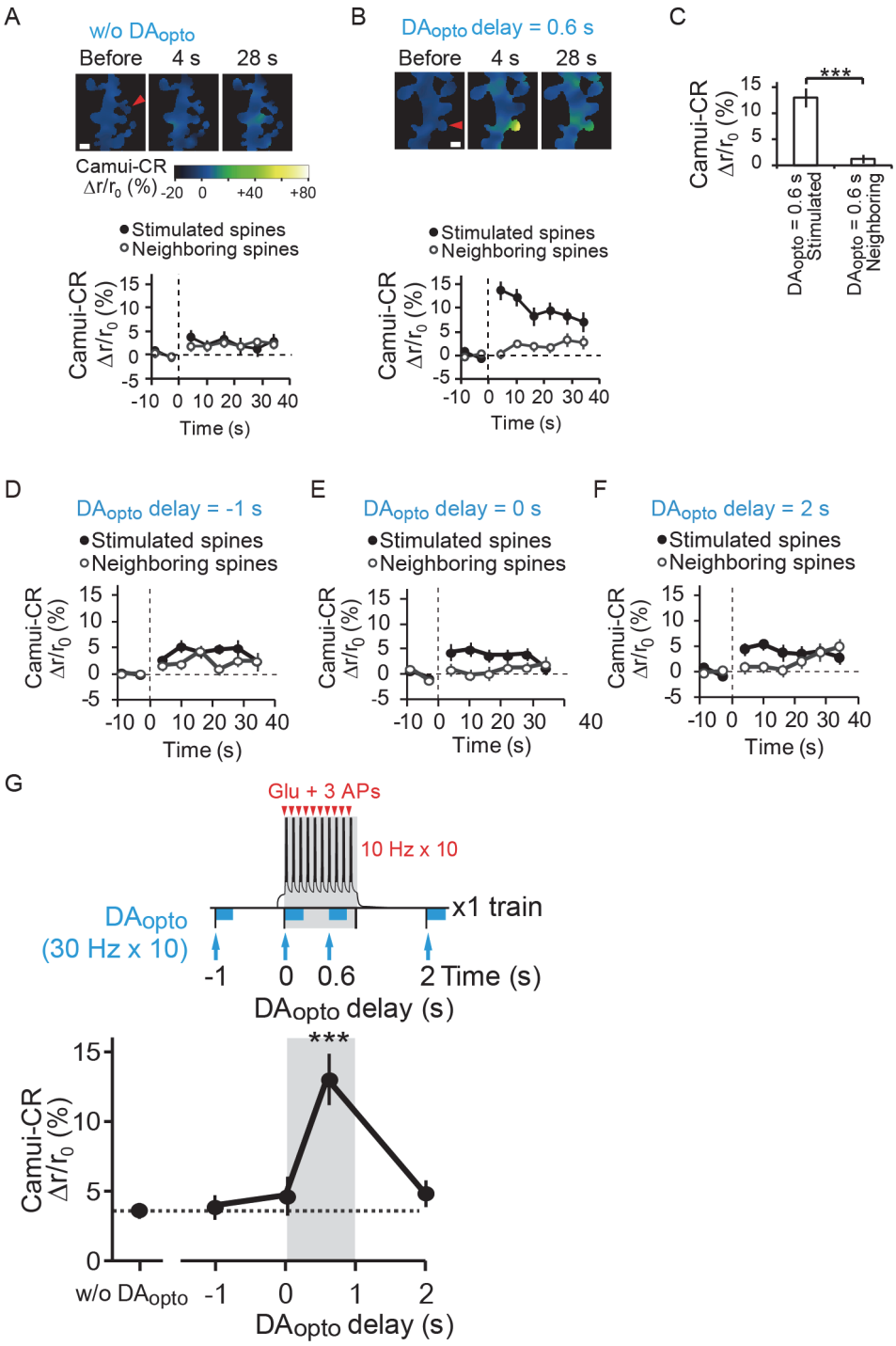

Fig. 8. DA_{opto} effects on STDP stimulation-induced increases in CaMKII activities. (**A**, **B**) Ratiometric imaging with Camuiα-CR during STDP stimulation in the absence (A, 33 spines, 14 dendrites) or presence of DA_{opto} with a 0.6-s delay (B, 42 spines, 14 dendrites). Relative increases in the ratio are shown as pseudocolor coding in (A). Lower panels show time courses of FRET ratios in the spines stimulated with glutamate

uncaging or the neighboring spines. Scale bars, 1 μm. (**C**) Normalized increases in Camuiα-CR ratios by STDP + DA_{opto} with a 0.6-s delay in the stimulated (42 spines, 14 dendrites) and neighboring spines (42 spines, 14 dendrites). Data are presented as mean ± s.e.m. Mann Whitney U test. *** $P = 3.2 \times 10^{-8}$ (**D-F**) Time courses of FRET ratios in the spines stimulated with glutamate uncaging or the neighboring spines during STDP + DA_{opto} with delays of –1 s (D, 32 spines, 8 dendrites), 0 s (E, 35 spines, 9 dendrites), and 2 s (F), 38 spines, 6 dendrites). (**G**) Increase in Camuiα-CR FRET ratios plotted versus DA_{opto} delay. $P = 1.3 \times 10^{-5}$ with Kruskal–Wallis test and ***$P = 8.4 \times 10^{-5}$ with Steel test vs. those without DA_{opto}.

How did dopamine activate CaMKII? Protein phosphatase-1 (PP-1) is expressed rich in dendritic spines of MSNs (Ouimet et al., 1995) and PP-1 is potently inhibited by dopamine- and cAMP-regulated phosphoprotein 32 kDa (DARPP-32) (Hemmings et al., 1984), which is activated by D1R/PKA pathway in D1R-MSNs (Bateup et al., 2008). Thus, I hypothesized that PKA/DARPP-32 would disinhibit CaMKII via PP-1 for the spine enlargement, similarly to hippocampal preparations (Blitzer et al., 1998). To test this hypothesis, I included an inhibitory peptide that blocks the interaction of DARPP-32 with PP-1 in the patch pipette (100 μM) (Kwon et al., 1997). DARPP-32 inhibitory peptide inhibited Camuiα-CR activation by STDP stimulation with DA_{opto} (Fig. 9A). The effect of inhibitory peptide was significant when compared to the condition in the absence of inhibitory peptide (Fig. 9B). The inhibitory peptide, but not its control peptide (100 μM in the pipette), prevented spine enlargement (Fig. 9C, D). These results suggest that DA_{opto} enhanced CaMKII activity and spine enlargement through the activation of DARPP-32.

Because DARPP-32 inhibits PP-1 activity (Hemmings et al., 1984), the above hypothesis predicted that PP-1 inhibition would mimic the effect of DA_{opto} on CaMKII activation. To test this, phosphoprotein phosphatase inhibitors were bath applied while spines were stimulated by STDP protocol in the absence of DA_{opto}. With PP-1/PP-2A

inhibitor (50 nM calyculin A whose IC_{50} values are 2 nM and 1 nM for PP-1 and PP-2A) (Ishihara et al., 1989), STDP stimulation resulted in CaMKII activation (Fig. 9E) and the inhibitor significantly increased CaMKII activation compared to the conditions in the absence of the inhibitor (Fig. 9F). Spine enlargement was also induced even in the absence of DA_{opto} when calyculin A was bath applied (Fig. 9G, H). Moreover, PP-1 specific inhibitor (4 nM tautomycetin whose IC_{50} values are 1.6 nM and 62 nM for PP-1 and PP-2A) replicated the result for CaMKII activation (Fig. 9E, F). Thus, PP-1 inhibition was enough to activate CaMKII and possibly to enhance spine enlargement. Collectively, the results from DARPP-32 inhibition and phosphatase inhibition were consistent with the hypothesis that PKA disinhibits CaMKII through PKA/DARPP-32/PP-1 pathway. Because CaMKII activity was DA_{opto}-timing dependent (Fig. 8G), I expected that PKA pathway that regulated CaMKII would be also sensitive to DA_{opto} timing.

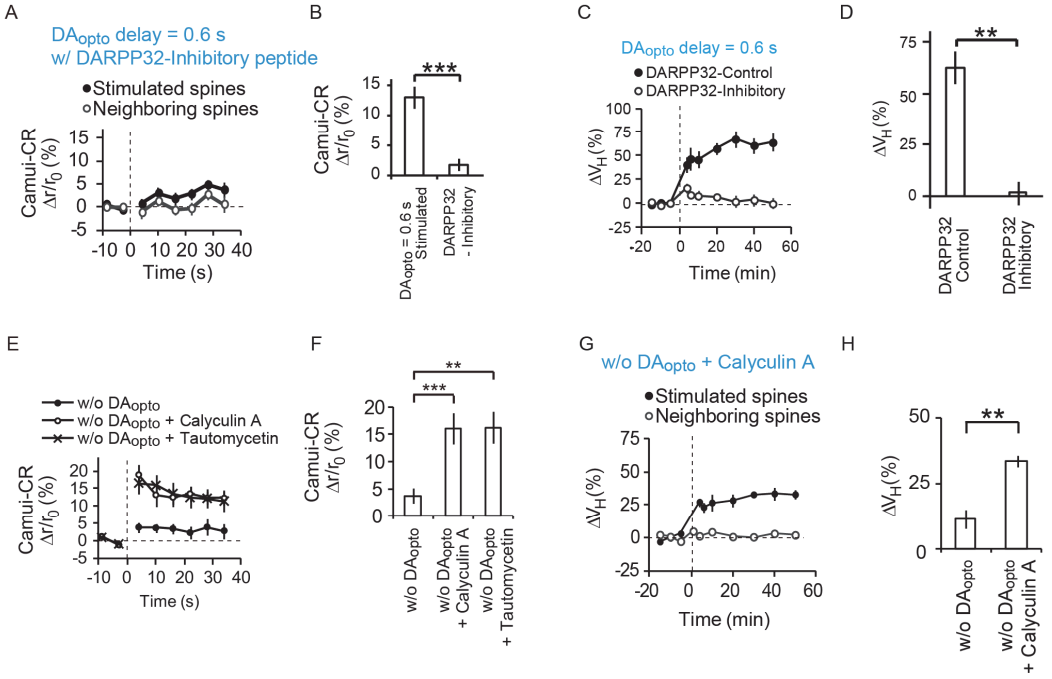

Fig. 9. DA_{opto} effects on CaMKII activities and structural plasticity depended on DARPP-32 and PP-1.

(**A**) Camuiα-CR responses to a single train of STDP + DA_{opto} with a delay of 0.6s in the presence of DARPP-32 inhibitory peptide (43 spines, 10 dendrites). (**B**) DARPP-32 inhibitory peptide blocked Camuiα-CR responses in comparison with the condition without peptide (Fig. 8C). Mann Whitney U test, *** $P = 5.6 \times 10^{-7}$. (**C**) Time courses of spine enlargement in the presence of inhibitory (100 μM, in the pipette, 24 spines, 6 dendrites) or control peptide for DARPP-32 (100 μM, in the pipette, 24 spines, 6 dendrites). (**D**) Averaged volume changes in the presence of DARPP-32 control peptide or DARPP-32 inhibitory peptide. Mann Whitney U test, ** $P = 0.0039$ (**E**) Camuiα-CR responses to a single train of STDP without DA_{opto} in the absence (16 spines, 4 dendrites) and the presence of PP-1 inhibitors, calyculin A (50 nM, 20 spines, 5 dendrites) or tautomycetin (4 nM, 22 spines, 5 dendrites). (**F**) The peak responses of Camuiα-CR ratios in the absence and presence of PP-1 inhibitors. $P = 0.0002$ with Kruskal–Wallis and ***$P = 0.0003$ (calyculin A) and ** $P = 0.0010$ (tautomycetin) by Steel test vs. that in the absence of inhibitor. (**G**) Time courses of spine enlargement induced by STDP without DA_{opto} in the presence of PP-1 inhibitor calyculin A (50 nM, 20 spines, 5 dendrites). (**H**) Effect of PP-1 inhibitor on spine volume change induced by STDP stimulation without DA_{opto}. Control value was derived from Fig 2D. Mann Whitney U test, ** $P = 0.0031$. Data are presented as mean ± s.e.m.

Thus, I addressed whether the DA_{opto} timing was formed at the level of PKA activation by using a FRET probe of PKA, AKAR2-CR (Lam et al., 2012), which was virally delivered to the D1R-MSNs. STDP and DA_{opto} were applied to the single spine and AKAR2-CR signals in the stimulated spine and neighboring spine were recorded (Fig. 10A-C). As a result, AKAR2-CR activation in the stimulated spine and the neighboring spine were not significantly different (Fig. 10D). Thus, unlike structural plasticity or Camuiα-CR activation, AKAR2-CR activation was not restricted to the stimulated spines. Even without glutamate uncaging, PKA activation was observed in the spine and dendritic shaft (Fig. 10E, F) in an AP-dependent manner (Fig. 10G), suggesting that PKA activation is a cell-wide phenomenon. When DA_{opto} was applied at various delays of −1 s (Fig. 10H), 0 s (Fig. 10I), 0.3 s (Fig. 10J), 1 s (Fig. 10K), 2 s (Fig. 10L) relative to APs, I obtained a timing (Fig. 10M) similar to DA_{opto} timing on spine enlargement and CaMKII activation (Fig. 3K, Fig. 8G). These results indicate that DA_{opto} and APs synergistically activate PKA activity.

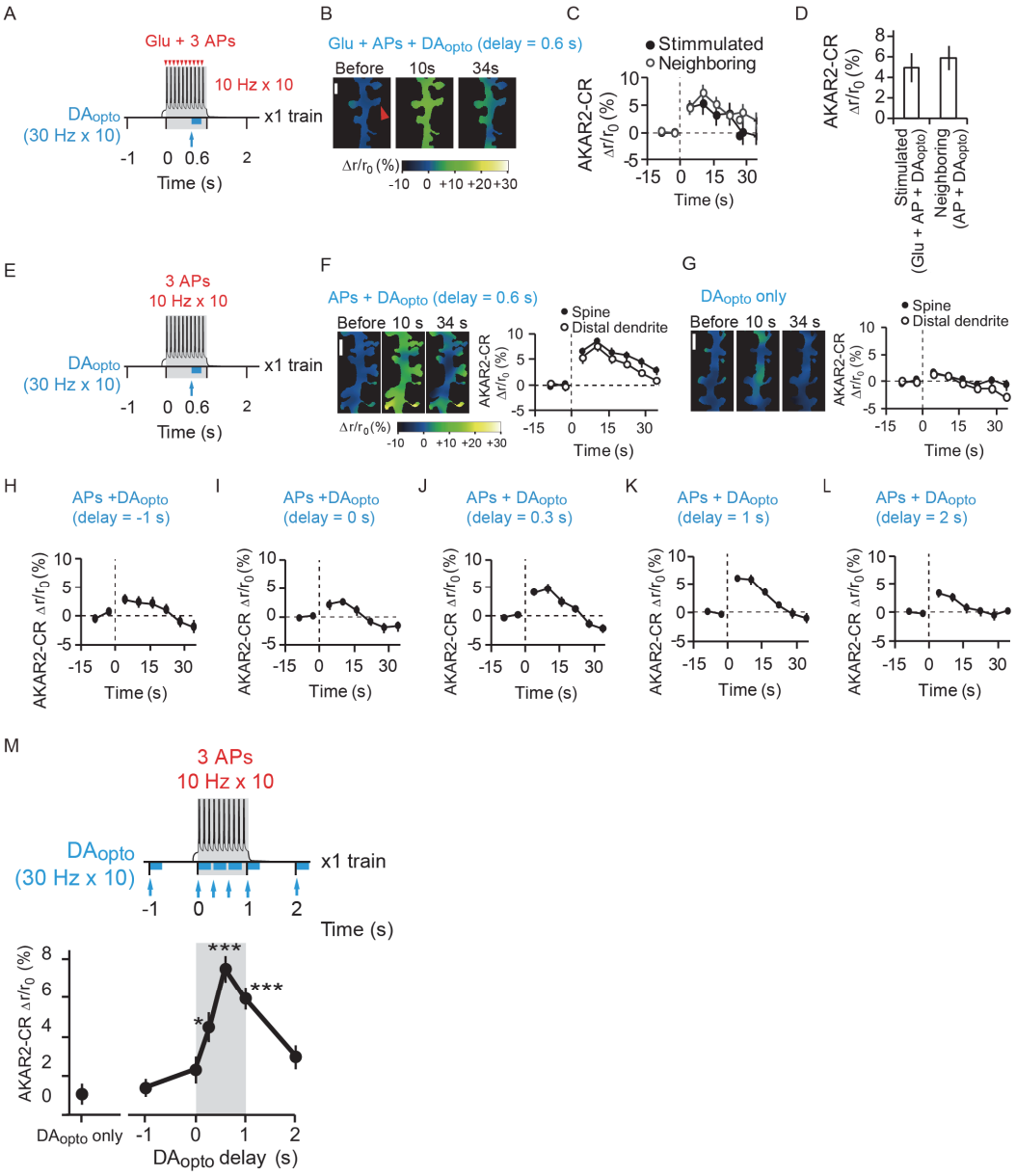

Fig. 10. DA_{opto} effects on STDP stimulation-induced and APs-induced increases in PKA activities.

(**A**) One train of STDP + DA_{opto} with a 0.6-s delay to measure PKA activation. (**B**) Images of FRET ratios of AKAR2-CR. A red arrowhead denotes the spine stimulated by caged glutamate. Scale bar, 1 μm. (**C**) The time courses of the ratios in stimulated and neighboring spines (36 spines, 21 dendrites). (**D**) Effects of glutamate uncaging on the AKAR2-CR signals. Both stimulated and neighboring spines showed significant increases in the AKAR2-CR signals compared with baseline. $P = 0.011$ (stimulated) and 1.6×10^{-6} (neighboring) with Mann-Whitney U test. There was no significant difference

between them. $P = 0.73$ with Mann-Whitney U test. (**E**) One train of APs + DA_{opto} with a 0.6-s delay to measure PKA activation. (**F, G**) Images and time courses of FRET ratios of AKAR2-CR in the spine and distal dendrites stimulated by APs + DA_{opto} with a 0.6-s delay (F, 153 spines, 25 dendrites) or DA_{opto} only (G, 158 spines, 26 dendrites). The relative increases in the ratio were pseudocolor coded as shown in (A). Scale bar, 2 μm. (**H–M**) AKAR2-CR responses to APs + DA_{opto} with various delays. Time courses of AKAR2-CR response to APs + DA_{opto} with delays of –1 s (H, 103 spines, 15 dendrites), 0 s (I, 116 spines, 18 dendrites), 0.3 s (J, 85 spines, 12 dendrites), 1 s (K, 81 spines, 11 dendrites), and 2 s (L, 104 spines, 16 dendrites). Increase in AKAR2-CR FRET ratios plotted versus DA_{opto} delay (M). $P = 5.3 \times 10^{-10}$ with Kruskal–Wallis test and $*P = 0.012$, $***P = 1.3 \times 10^{-6}$ (0.6 s) and 4.0×10^{-4} (1 s) with Steel test vs. DA_{opto} only.

APs themselves were not sufficient to activate PKA (Fig. 11A–C). The coincidence of DA_{opto} and APs might be detected by Ca^{2+}/calmodulin dependent adenylyl cyclase 1 (AC1), which is synergistically activated by Ca^{2+}/calmodulin and Gs (Ferguson and Storm, 2004). To test this, I included AC1 blocker (50 μM NB001 in the pipette) into the patch pipette. AC1 blocker significantly inhibited AKAR2 activation (Fig. 12A–B) and structural plasticity (Fig. 12C–D), compared to the conditions in the absence of NB001 (Fig. 3G, Fig. 10F).

In contrast to the distal dendrites, DA_{opto} alone was sufficient to activate PKA in the soma and proximal (first branch) dendrites (Fig. 13A–D), consistent with previous finding recorded PKA activity in soma from MSNs (Castro et al., 2013). APs could only slightly enhance PKA (Fig. 13D), suggesting that DA_{opto} timing is less important in soma for PKA activation. The extent of spine enlargement positively correlated with that of PKA activation in spine (Fig. 13C). I predict that APs might have modulated spine enlargement to a small degree in these regions, if there had been spines (Fig. 13C). Thus, DA_{opto}-induced PKA activation must be suppressed in distal dendrites to attain the large dynamic range and the sequence detection.

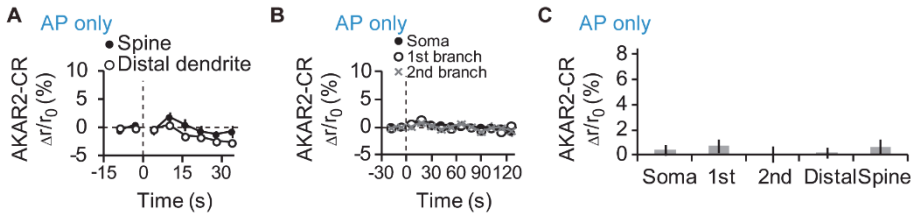

Fig. 11. **PKA activities induced by APs**

(**A**, **B**) AP-induced AKAR2-CR responses at the spine and distal dendrites (A, 100 spines, 16 dendrites) and in the soma and first and second dendrite branches (B, 14 soma/dendrites). None of them showed significant increases in the AKAR2-CR signals compared with baseline. P = 0.49 (soma), 0.49 (first), 0.17 (second), 1.0 (distal), and 0.053 (spine) with Mann-Whitney U test (not corrected for multiple comparisons). Data are presented as mean ± s.e.m. (**C**) Averaged increases in AKAR2-CR signals in the conditions shown in (A, B).

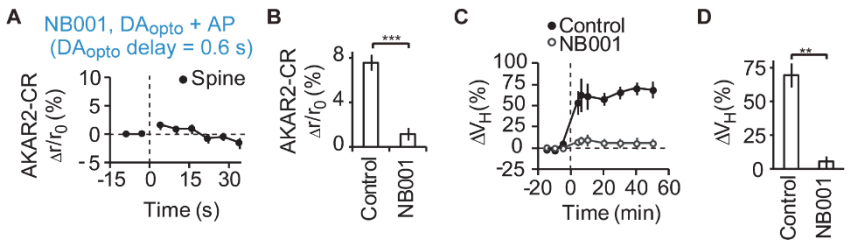

Fig. 12. **Effect of AC1 blocker on PKA activities.**

(**A**) Time courses of AKAR2-CR activation by AP + DA_{opto} with a 0.6-s delay in the presence of NB001 (50 μM). (**B**) The peak FRET signals of AKAR2-CR in the absence (153 spines, 25 dendrites, the same data as Fig. 4a) and presence of NB001 (50 μM, 151 spines, 22 dendrites). ***$P = 4.3 \times 10^{-7}$ with Mann-Whitney U test. (**C**)Time courses of spine enlargement induced by STDP + DA_{opto} in the absence (24 spines, 7 dendrites, the same data as Fig. 2a, Control) and presence of NB001 (23 spines, 6 dendrites). (**D**)

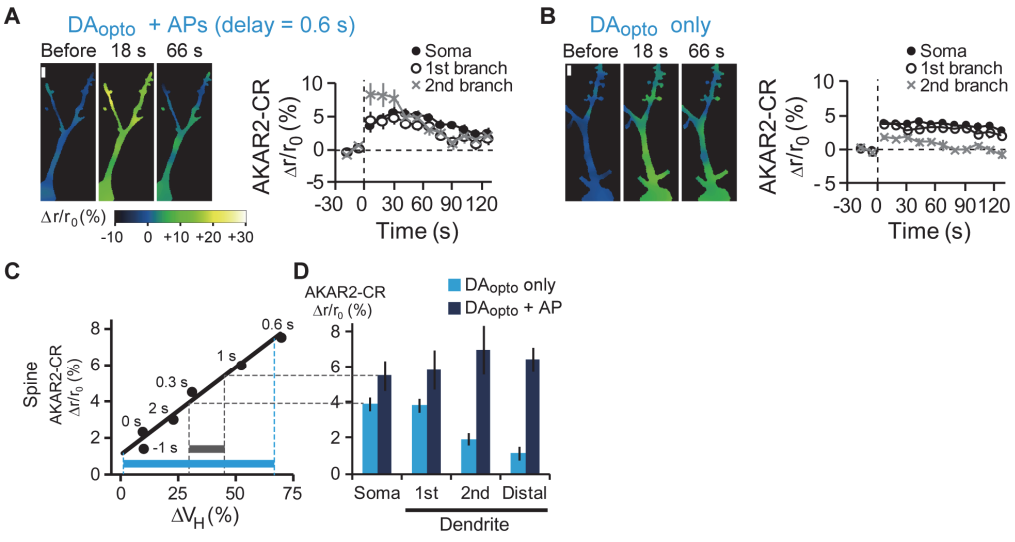

Fig. 13. Subcellular difference in PKA signaling in response to DA_{opto}.

(**A, B**) Time-course of AKAR2-CR responses at the soma and first and second dendrite branches stimulated by APs + DA_{opto} with a 0.6-s delay (A, 11 soma/dendrites) or DA_{opto} only (B, 25 soma/dendrites). DA_{opto} only did not induce significant activation in distal dendrites compared with baseline (P = 0.12, 26 dendrites, Mann-Whitney U test). There was a significant effect of subcellular region on AKAR2-CR responses to DA_{opto} only ($P = 4.1 \times 10^{-6}$, Kruskal–Wallis test), and the soma and first branch showed significantly greater responses compared with distal dendrites. P = 0.0002 (soma) and 0.0003 (first) with Steel's test. Scale bar, 2 µm. (**C**) AKAR2-CR response in spine (Fig. 10N) plotted versus spine volume changes (Fig. 3K) for various DA_{opto} timings. The Spearman's correlation coefficient was 0.94, and P = 0.0048. The blue and grey bars indicate the dynamic ranges of volume changes predicted by the dynamic ranges of AKAR2 responses at dendritic spine (blue) and soma (grey). (**D**) AKAR2-CR responses at the soma and first, second, and distal dendrites in response to DA_{opto} only and DA_{opto} + APs with a 0.6-s delay.

In fact, when phosphodiesterase 10A (PDE10A), the major phosphodiesterase in MSNs, was blocked by its inhibitor papaverine (Nishi et al., 2008), PKA activations were similarly induced in distal dendrites as in the soma (Fig. 14A–C). In the presence of papaverine, STDP with DA_{opto} delay of 0 s and 2 s as well as 0.6 s caused spine enlargement (Fig. 14D). Thus, papaverine disrupted the time window for structural plasticity (Fig. 14E).

Why were PDE10A actions particularly potent in the distal dendrites? Subcellular differences in PDE10A expression might not account for this, considering that PDE10A is expressed at the plasma membrane and is uniformly distributed along the dendrites (Charych et al., 2010). Instead, I found a negative correlation between dendrite diameter and DA_{opto}-induced PKA activity (Fig. 15A, blue) which was lost when the phosphodiesterase was inhibited (Fig. 15A, orange). Therefore, PDE10A might counteract the increases in cAMP more potently in the thin distal dendrites because of its high surface-to-volume ratios (Fig. 15A–C). Spines are only found in the distal thin dendrites of MSNs (Fig. 15B–E) (Wilson and Groves, 1980), suggesting that spines are distributed to be efficiently modulated by dopamine timing in MSNs.

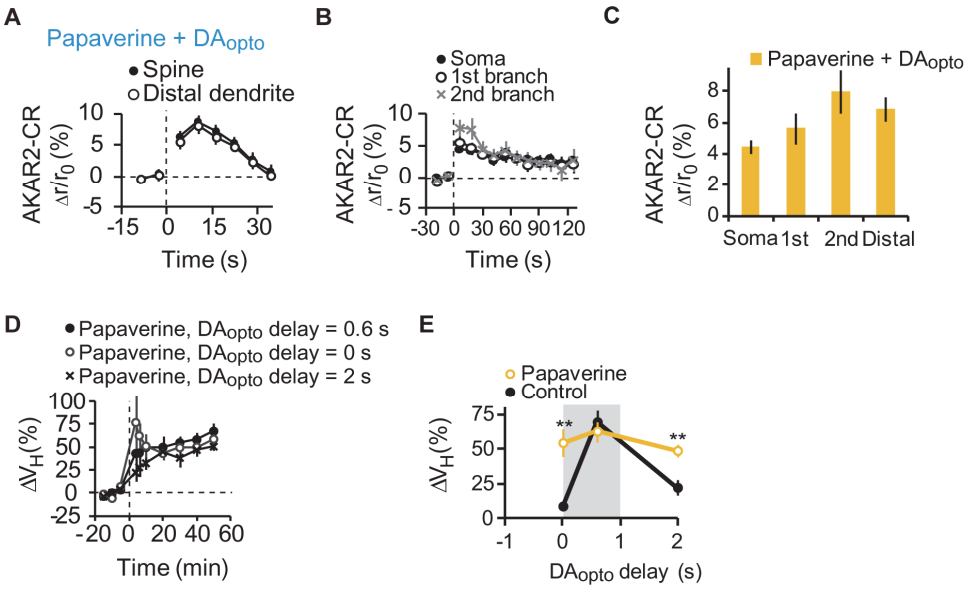

Fig. 14. Effects of phosphodiesterase inhibitor on PKA activities and spine enlargement.

(**A**, **B**) The time courses of DA_{opto} -induced AKAR2-CR FRET signals in the presence of papaverine in spines and distal dendrites (A, 143 spines, 22 dendrites), and the soma and first and second dendrite branches (B, 9 soma/dendrites). (**C**) AKAR2 responses to DA_{opto} in the presence of the PDE10A inhibitor papaverine. They were not dependent on subcellular regions (P = 0.09, Kruskal–Wallis test). (**D**) The traces of spine enlargement induced by STDP and DA_{opto} with delays of 0.6 s (23 spines, 6 dendrites), 0 s (24 spines, 6 dendrites), or 2 s (24 spines, 6 dendrites) in the presence of papaverine. (**E**) Papaverine effects on DA_{opto} timing on spine enlargement. $^{**}P$ = 0.0011 (0 s) and 0.0066 (2 s), Mann-Whitney U test vs. the control values derived from Fig. 3K. Data are presented as mean ± s.e.m.

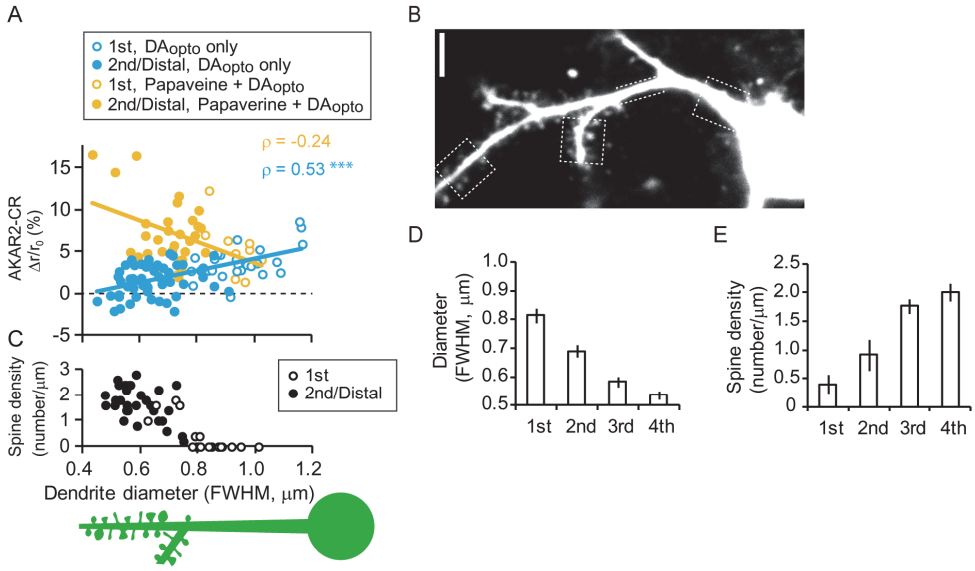

Fig. 15. Dendritic diameters and spine densities in MSNs.

(**A**) Dependence of DA_{opto}-evoked AKAR2-CR signals on dendritic diameters quantified by full-width-at-half-maximal (FWHM) diameters. The Spearman's correlation coefficients were ρ = 0.53 (***$P = 7.6 \times 10^{-7}$, 76 dendrites) in control, and ρ = –0.24 ($P = 0.13$, 40 dendrites) in the presence of papaverine. (**B**) A representative image of an MSN that was whole-cell perfused with Alexa 488. Scale bar, 5 μm. The dotted boxes indicate the first, second, third, and fourth branches of dendrites. (**C**, **D**) Average diameters (C) and spine density (D) of dendrites for each branch (51 dendritic branches, 6 cells). (**E**) The spine densities along MSN dendrites. Spines were only present in dendrites thinner than 0.8 μm, as illustrated in the diagram.

Discussion

It has been enigmatic why dopamine reinforces preceding, but not subsequent, sensorimotor events. If dopamine always activates PKA, its effects should last long enough to reinforce the subsequent events over tens of seconds (Fig. 10C, F). However, dopamine did not activate PKA unless $[Ca^{2+}]_i$ primed AC1 to outcompete the high phosphodiesterase activity in thin dendrites (Fig. 16). My data show that $[Ca^{2+}]_i$ priming should occur strictly before dopamine delivery (Fig. 3K, 8H, 10N; 0 s), which is reminiscent of serotonin's action in the classical conditioning of the siphon withdrawal reflex in *Aplysia* (Hawkins et al., 1983), where serotonin, carrying an aversive signal, was only effective when it was preceded by increases in $[Ca^{2+}]_i$ for activation of calcium-dependent adenylyl cyclase (AC) and PKA in presynaptic terminals (Yovell and Abrams, 1992). The delayed actions of $[Ca^{2+}]_i$ on AC may compensate the time lag of monoaminergic signals after reward or punishment, and are due to a delay in $[Ca^{2+}]_i$ priming of AC1. My data suggest that reinforcement plasticity occurs at the single spine level, even though PKA activation is a cell-wide phenomenon, in such a way that dopamine regulates the gain of NMDAR-dependent Hebbian plasticity via CaMKII activity (Fig. 16). This interdependence between Hebbian and reinforcement plasticity has been implicitly assumed in the reinforcement learning theory, where the Hebbian

term is used for the credit assignment (Schultz, 1998; Sutton and Barto, 1998), and the dopamine timing in my study corresponds to the eligibility trace that determines the time window for reward action (Sutton and Barto, 1998).

Similar time windows for monoamines to modulate plasticity were recently reported from other groups. In the olfactory tubercle, optogenetic stimulation of dopamine fibers enhanced synaptic plasticity of MSNs only when applied within 1 s from electrical stimulation of glutamatergic fibers (Wieland et al., 2015), consistent with my result. In the neocortex, serotonin and noradrenaline modulated plasticity within the time window of 2 to 5 s (He, 2015). Therefore, it is highly plausible that at the synapse level, glutamatergic and monoaminergic signals should be coincided within a few seconds for the modulation of plasticity.

In a previous behavioral study, a similar narrow time window for conditioned learning was observed when dopaminergic fiber was electrically stimulated (Black et al., 1985). Our unpublished data also showed that in the Pavlovian conditioning where tone and reward were given to the head-fixed mice, the time window for conditioning was close to the time window for the plasticity. This Pavlovian conditioning was rapidly formed within 10 min (50 trials) in NAc dependent manner. In contrast, more extended training periods, usually several days, allow animals to associate the reward with longer

delays (~20 s) in complex behavioral paradigms (Bersh, 1951; Boice and Denny, 1965; Miyazaki et al., 2012; Howe et al., 2013; Miyazaki et al., 2014). These forms of learning with delayed reward might involve other brain regions. For example, the hippocampal lesion impairs reward learning in delayed matching/non- matching tasks (Rawlins and Tanner, 1998; Hampson et al., 1999; Savage et al., 2004). The orbitofrontal cortex is also suggested to process delayed rewards (Roesch et al., 2006; Jocham et al., 2016). Therefore, the brain might use several mechanisms for learning depending on the situation and the reinforcement plasticity in NAc might play a major role for rapid learning when rewarded immediately (Hariri et al., 2006).

It remains open whether MSNs in the dorsal striatum have a similar time window to MSNs in NAc. Even if a similar time window exists, its role in the learning would be different. While NAc is essential for Pavlovian reward learning in which the animal associates sensory information with reward (Smith-Roe and Kelley, 2000; Roitman et al., 2005; Darvas et al., 2014), dorsal striatum is involved in learning to adjust motor actions (Graybiel et al., 1994; Tai et al., 2012; Cui et al., 2013). A recent study showed that dopamine terminals in NAc responded to reward and reward-predicting sensory events whereas dopamine terminals in the dorsal striatum responded to motor events (Parker et al., 2016).

The principle neurons in the striatum consist of D1R-MSNs constituting the direct pathway and D2R-MSNs constituting the indirect pathway. As discussed in this paper, D1R-MSNs were involved in reward-related learning whereas D2R-MSNs contributed to the aversive learning in response to punishment (Hikida et al., 2010; Nakanishi et al., 2014). At the cellular level, D2R has been considered to detect decrease in the dopamine concentration induced by punishment and resultant inactivation of D2R is thought to disinhibit downstream Gi/o to activate PKA (Nakanishi et al., 2014). Consistent with this idea, recent optogenetic studies have shown that transient inhibitions of dopamine neurons were sufficient to cause aversive learnings (Danjo et al., 2014; Chang et al., 2015; Eshel et al., 2015). Thus, it would be interesting to test whether D2R-MSNs have an ability to detect dopamine punishment signal in timing dependent manner.

In conclusion, I have clarified a molecular and cellular basis of reinforcement plasticity at the level of single dendritic spines. This could provide a new research focus for psychiatric disorders with dopaminergic dysfunction, such as schizophrenia, depression and addiction.

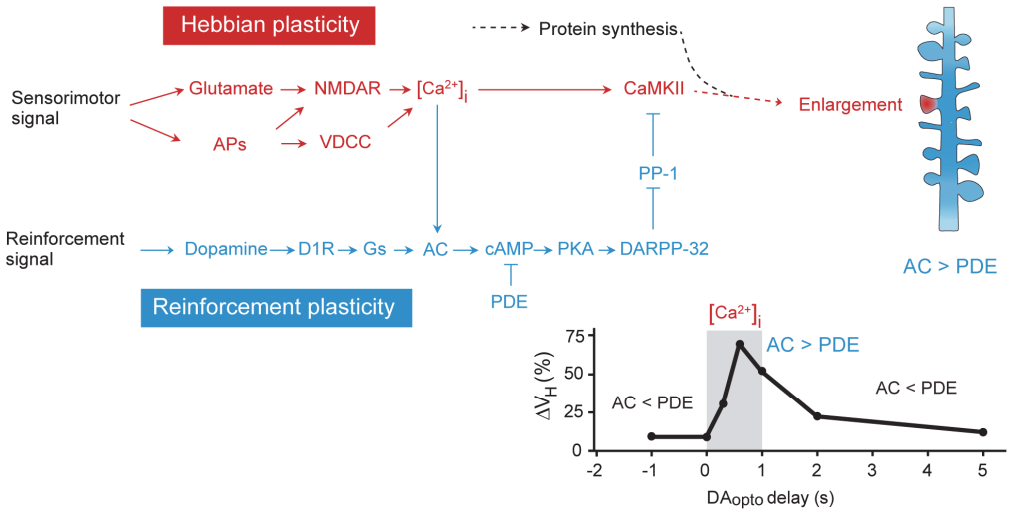

Fig. 16. A signaling scheme for Hebbian and reinforcement plasticity in synaptic spines.

Signaling cascades for reinforcement and Hebbian plasticity of dendritic spines in MSNs. Concurrent activation of presynaptic inputs (glutamate) and postsynaptic APs results in Ca^{2+} influx through NMDARs that stimulate CaMKII. This Hebbian mechanism is not sufficient to fully activate CaMKII; rather, it requires reinforcement by PKA-DARPP-32-PP1 signaling. PKA activation requires APs and subsequent dopamine to overcome the high phosphodiesterase activity in thin distal dendrites. Thus, the balance of activity between phosphodiesterase and Ca^{2+}-dependent adenylate cyclase shapes the temporal window for dopamine's effects on PKA activation and spine enlargement. Because these molecules are expressed in synaptic spines in various brain regions, analogous mechanisms may occur throughout the brain, particularly in those neurons with spines and thin dendrites (Fig. 13C, D).

References

Backman CM, Malik N, Zhang Y, Shan L, Grinberg A, Hoffer BJ, Westphal H, Tomac AC (2006) Characterization of a mouse strain expressing Cre recombinase from the 3' untranslated region of the dopamine transporter locus. Genesis 44: 383-390.

Bateup HS, Svenningsson P, Kuroiwa M, Gong S, Nishi A, Heintz N, Greengard P (2008) Cell type-specific regulation of DARPP-32 phosphorylation by psychostimulant and antipsychotic drugs. Nature Neuroscience 11: 932-939.

Bersh PJ (1951) The influence of two variables upon the establishment of a secondary reinforcer for operant responses. Journal of Experimental Psychology 41: 62-73.

Black J, Belluzzi JD, Stein L (1985) Reinforcement delay of one second severely impairs acquisition of brain self-stimulation. Brain Research 359: 113-119.

Blitzer RD, Connor JH, Brown GP, Wong T, Shenolikar S, Iyengar R, Landau EM (1998) Gating of CaMKII by cAMP-regulated protein phosphatase activity during LTP. Science 280: 1940-1942.

Boice R, Denny MR (1965) The conditioned licking response in rats as a function of the CS-UCS interval. Psychonomic Science 3: 93-94.

Calabresi P, Gubellini P, Centonze D, Picconi B, Bernardi G, Chergui K, Svenningsson P, Fienberg AA, Greengard P (2000) Dopamine and cAMP-regulated phosphoprotein 32 kDa controls both striatal long-term depression and long-term potentiation, opposing forms of synaptic plasticity. Journal of Neuroscience 20: 8443-8451.

Castro LRV, Brito M, Guiot E, Polito M, Korn CW, Herve D, Girault JA, Paupardin-Tritsch D, Vincent P (2013) Striatal neurones have a specific ability to respond to phasic dopamine release. Journal of Physiology 591: 3197-3214.

Cepeda C, Levine MS (2006) Where do you think you are going? The NMDA-D1 receptor trap. Science's STKE 2006 333: 20.

Chang CY, Esber GR, Marrero-Garcia Y, Yau HJ, Bonci A, Schoenbaum G (2016) Brief optogenetic inhibition of dopamine neurons mimics endogenous negative reward prediction errors. Nature Neuroscience 19: 111-116.

Charych EI, Jiang LX, Lo F, Sullivan K, Brandon NJ (2010) Interplay of palmitoylation and phosphorylation in the trafficking and localization of phosphodiesterase 10A: implications for the treatment of schizophrenia. Journal of Neuroscience 30: 9027-9037.

Chen Q, Veenman L, Knopp K, Yan Z, Medina L, Song WJ, Surmeier DJ, Reiner A (1998) Evidence for the preferential localization of glutamate receptor-1 subunits of AMPA receptors to the dendritic spines of medium spiny neurons in rat striatum. Neuroscience 83: 749-761.

Cohen JY, Haesler S, Vong L, Lowell BB, Uchida N (2012) Neuron-type-specific signals for reward and punishment in the ventral tegmental area. Nature 482: 85-88.

Corder G, Doolen S, Donahue RR, Winter MK, Jutras BL, He Y, Hu X, Wieskopf JS, Mogil JS, Storm DR, Wang ZJ, McCarson KE, Taylor BK (2013) Constitutive mu-opioid receptor activity leads to long-term endogenous analgesia and dependence. Science 341: 1394-1399.

Cui G, Jun SB, Jin X, Pham MD, Vogel SS, Lovinger DM, Costa RM (2013) Concurrent activation of striatal direct and indirect pathways during action initiation. Nature 494: 238-242.

Dan Y, Poo MM (2006) Spike timing-dependent plasticity: from synapse to perception. Physiological Review 86: 1033-1048.

Danjo T, Yoshimi K, Funabiki K, Yawata S, Nakanishi S (2014) Aversive behavior induced by optogenetic inactivation of ventral tegmental area dopamine neurons

is mediated by dopamine D2 receptors in the nucleus accumbens. Proceedings of the National Academy of Sciences of the United States of America 111: 6455-6460.

Darvas M, Wunsch AM, Gibbs JT, Palmiter RD (2014) Dopamine dependency for acquisition and performance of Pavlovian conditioned response. Proceedings of the National Academy of Sciences of the United States of America 111: 2764-2769.

Day JJ, Roitman MF, Wightman RM, Carelli RM (2007) Associative learning mediates dynamic shifts in dopamine signaling in the nucleus accumbens. Nature Neuroscience 10: 1020-1028.

Ellis-Davies GC, Matsuzaki M, Paukert M, Kasai H, Bergles DE (2007) 4-Carboxymethoxy-5,7-dinitroindolinyl-Glu: an improved caged glutamate for expeditious ultraviolet and two-photon photolysis in brain slices. Journal of Neuroscience 27: 6601-6604.

Eshel N, Bukwich M, Rao V, Hemmelder V, Tian J, Uchida N (2015) Arithmetic and local circuitry underlying dopamine prediction errors. Nature.

Ferguson GD, Storm DR (2004) Why calcium-stimulated adenylyl cyclases? Physiology 19: 271-276.

Gerfen CR, Engber TM, Mahan LC, Susel Z, Chase TN, Monsma FJ, Jr., Sibley DR (1990) D1 and D2 dopamine receptor-regulated gene expression of striatonigral and striatopallidal neurons. Science 250: 1429-1432.

Gracy KN, Pickel VM (1996) Ultrastructural immunocytochemical localization of the N-methyl-D-aspartate receptor and tyrosine hydroxylase in the shell of the rat nucleus accumbens. Brain Research 739: 169-181.

Graybiel AM, Aosaki T, Flaherty AW, Kimura M (1994) The basal ganglia and adaptive motor control. Science 265: 1826-1831.

Grieger JC, Choi VW, Samulski RJ (2006) Production and characterization of adeno-associated viral vectors. Nature Protocols 1: 1412-1428.

Hampson RE, Jarrard LE, Deadwyler SA (1999) Effects of ibotenate hippocampal and extrahippocampal destruction on delayed-match and -nonmatch-to-sample behavior in rats. Journal of Neuroscience 19: 1492-1507.

Hara Y, Pickel VM (2005) Overlapping intracellular and differential synaptic distributions of dopamine D1 and glutamate N-methyl-D-aspartate receptors in rat nucleus accumbens. Journal of Comparative Neurology 492: 442-455.

Hariri AR, Brown SM, Williamson DE, Flory JD, de Wit H, Manuck SB (2006) Preference for immediate over delayed rewards is associated with magnitude of ventral striatal activity. Journal of Neuroscience 26: 13213-13217.

Harvey CD, Yasuda R, Zhong H, Svoboda K (2008) The spread of Ras activity triggered by activation of a single dendritic spine. Science 321: 136-140.

Hawkins RD, Abrams TW, Carew TJ, Kandel ER (1983) A cellular mechanism of classical conditioning in Aplysia: activity-dependent amplification of presynaptic facilitation. Science 219: 400-405.

He K, Huertas M, Hong SZ, Tie XX, Hell JW, Shouval H, Kirkwood A (2015) Distinct Eligibility Traces for LTP and LTD in Cortical Synapses. Neuron 88: 528-538.

Hemmings HC, Greengard P, Tung HYL, Cohen P (1984) Darpp-32, a Dopamine-Regulated Neuronal Phosphoprotein, Is a Potent Inhibitor of Protein Phosphatase-1. Nature 310: 503-505.

Hikida T, Kimura K, Wada N, Funabiki K, Nakanishi S (2010) Distinct Roles of Synaptic Transmission in Direct and Indirect Striatal Pathways to Reward and Aversive Behavior. Neuron 66: 896-907.

Howe MW, Tierney PL, Sandberg SG, Phillips PE, Graybiel AM (2013) Prolonged dopamine signalling in striatum signals proximity and value of distant rewards. Nature 500: 575-579.

Ishihara H, Martin BL, Brautigan DL, Karaki H, Ozaki H, Kato Y, Fusetani N, Watabe S, Hashimoto K, Uemura D, et al. (1989) Calyculin A and okadaic acid: inhibitors of protein phosphatase activity. Biochemical and Biophysical Research Communications 159: 871-877.

Jocham G, Brodersen Kay H, Constantinescu Alexandra O, Kahn Martin C, Ianni AM, Walton Mark E, Rushworth Matthew FS, Behrens Timothy EJ (2016) Reward-Guided Learning with and without Causal Attribution. Neuron 90: 177-190.

Kwon YG, Huang HB, Desdouits F, Girault JA, Greengard P, Nairn AC (1997) Characterization of the interaction between DARPP-32 and protein phosphatase 1 (PP-1): DARPP-32 peptides antagonize the interaction of PP-1 with binding proteins. Proceedings of the National Academy of Sciences of the United States of America 94: 3536-3541.

Lam AJ, St-Pierre F, Gong YY, Marshall JD, Cranfill PJ, Baird MA, McKeown MR, Wiedenmann J, Davidson MW, Schnitzer MJ, Tsien RY, Lin MZ (2012)

Improving FRET dynamic range with bright green and red fluorescent proteins. Nature Methods 9: 1005-1012.

Lammel S, Steinberg EE, Foldy C, Wall NR, Beier K, Luo L, Malenka RC (2015) Diversity of transgenic mouse models for selective targeting of midbrain dopamine neurons. Neuron 85: 429-438.

Lee SJR, Escobedo-Lozoya Y, Szatmari EM, Yasuda R (2009) Activation of CaMKII in single dendritic spines during long-term potentiation. Nature 458: 299-304.

Matsuda Y, Marzo A, Otani S (2006) The presence of background dopamine signal converts long-term synaptic depression to potentiation in rat prefrontal cortex. Journal of Neuroscience 26: 4803-4810.

Matsuzaki M, Honkura N, Ellis-Davies GCR, Kasai H (2004) Structural basis of long-term potentiation in single dendritic spines. Nature 429: 761-766.

Matsuzaki M, Ellis-Davies GC, Nemoto T, Miyashita Y, Iino M, Kasai H (2001) Dendritic spine geometry is critical for AMPA receptor expression in hippocampal CA1 pyramidal neurons. Nature Neuroscience 4: 1086-1092.

Miyazaki KW, Miyazaki K, Doya K (2012) Activation of dorsal raphe serotonin neurons is necessary for waiting for delayed rewards. Journal of Neuroscience 32: 10451-10457.

Miyazaki KW, Miyazaki K, Tanaka KF, Yamanaka A, Takahashi A, Tabuchi S, Doya K (2014) Optogenetic activation of dorsal raphe serotonin neurons enhances patience for future rewards. Current Biology 24: 2033-2040.

Nakanishi S, Hikida T, Yawata S (2014) Distinct dopaminergic control of the direct and indirect pathways in reward-based and avoidance learning behaviors. Neuroscience 282: 49-59.

Nakano T, Yoshimoto J, Doya K (2013) A model-based prediction of the calcium responses in the striatal synaptic spines depending on the timing of cortical and dopaminergic inputs and post-synaptic spikes. Frontiers in Computational Neuroscience 7: 119.

Nishi A, Kuroiwa M, Miller DB, O'Callaghan JP, Bateup HS, Shuto T, Sotogaku N, Fukuda T, Heintz N, Greengard P, Snyder GL (2008) Distinct roles of PDE4 and PDE10A in the regulation of cAMP/PKA signaling in the striatum. Journal of Neuroscience 28: 10460-10471.

Ouimet CC, da Cruz e Silva EF, Greengard P (1995) The alpha and gamma 1 isoforms of protein phosphatase 1 are highly and specifically concentrated in dendritic spines. Proceedings of the National Academy of Sciences of the United States of America 92: 3396-3400.

Parker NF, Cameron CM, Taliaferro JP, Lee J, Choi JY, Davidson TJ, Daw ND, Witten IB (2016) Reward and choice encoding in terminals of midbrain dopamine neurons depends on striatal target. Nature Neuroscience *Advance online publication*.

Pavlov IP (1927) Conditioned reflexes; an investigation of the physiological activity of the cerebral cortex. Oxford University Press, London.

Rawlins JN, Tanner J (1998) The effects of hippocampal aspiration lesions on conditioning to the CS and to a background stimulus in trace conditioned suppression. Behavioral Brain Research 91: 61-72.

Rescorla RA (1988) Behavioral studies of Pavlovian conditioning. Annual Review of Neuroscience 11: 329-352.

Reynolds JNJ, Hyland BI, Wickens JR (2001) A cellular mechanism of reward-related learning. Nature 413: 67-70.

Roesch MR, Taylor AR, Schoenbaum G (2006) Encoding of time-discounted rewards in orbitofrontal cortex is independent of value representation. Neuron 51: 509-520.

Roitman MF, Wheeler RA, Carelli RM (2005) Nucleus accumbens neurons are innately tuned for rewarding and aversive taste stimuli, encode their predictors, and are linked to motor output. Neuron 45: 587-597.

Savage LM, Buzzetti RA, Ramirez DR (2004) The effects of hippocampal lesions on learning, memory, and reward expectancies. Neurobiology of Learning and Memory 82: 109-119.

Schultz W (1998) Predictive reward signal of dopamine neurons. Journal of Neurophysiology 80: 1-27.

Shen W, Flajolet M, Greengard P, Surmeier DJ (2008) Dichotomous dopaminergic control of striatal synaptic plasticity. Science 321: 848-851.

Smith-Roe SL, Kelley AE (2000) Coincident activation of NMDA and dopamine D1 receptors within the nucleus accumbens core is required for appetitive instrumental learning. Journal of Neuroscience 20: 7737-7742.

Stuber GD, Stamatakis AM, Kantak PA (2015) Considerations when using cre-driver rodent lines for studying ventral tegmental area circuitry. Neuron 85: 439-445.

Stuber GD, Hnasko TS, Britt JP, Edwards RH, Bonci A (2010) Dopaminergic terminals in the nucleus accumbens but not the dorsal striatum corelease glutamate. Journal of Neuroscience 30: 8229-8233.

Surmeier DJ, Plotkin J, Shen W (2009) Dopamine and synaptic plasticity in dorsal striatal circuits controlling action selection. Current Opinion in Neurobiology 19: 621-628.

Surmeier DJ, Carrillo-Reid L, Bargas J (2011) Dopaminergic modulation of striatal neurons, circuits, and assemblies. Neuroscience 198: 3-18.

Sutton RS, Barto AG (1998) Reinforcemnet learning. Cambridge: MIT Press.

Tai LH, Lee AM, Benavidez N, Bonci A, Wilbrecht L (2012) Transient stimulation of distinct subpopulations of striatal neurons mimics changes in action value. Nature Neuroscience 15: 1281-1289.

Takao K, Okamoto K, Nakagawa T, Neve RL, Nagai T, Miyawaki A, Hashikawa T, Kobayashi S, Hayashi Y (2005) Visualization of synaptic Ca2+ /calmodulin-dependent protein kinase II activity in living neurons. Journal of Neuroscience 25: 3107-3112.

Tanaka J, Horiike Y, Matsuzaki M, Miyazaki T, Ellis-Davies GC, Kasai H (2008) Protein synthesis and neurotrophin-dependent structural plasticity of single dendritic spines. Science 319: 1683-1687.

Tecuapetla F, Patel JC, Xenias H, English D, Tadros I, Shah F, Berlin J, Deisseroth K, Rice ME, Tepper JM, Koos T (2010) Glutamatergic signaling by mesolimbic dopamine neurons in the nucleus accumbens. Journal of Neuroscience 30: 7105-7110.

Thorndike EL (1911) Animal Intelligence. Macmillan, New York.

Tritsch NX, Ding JB, Sabatini BL (2012) Dopaminergic neurons inhibit striatal output through non-canonical release of GABA. Nature 490: 262-266.

Wang HS, Xu H, Wu LJ, Kim SS, Chen T, Koga K, Descalzi G, Gong B, Vadakkan KI, Zhang XH, Kaang BK, Zhuo M (2011) Identification of an Adenylyl Cyclase Inhibitor for Treating Neuropathic and Inflammatory Pain. Science Translational Medicine 3: 65.

Wieland S, Schindler S, Huber C, Kohr G, Oswald MJ, Kelsch W (2015) Phasic Dopamine Modifies Sensory-Driven Output of Striatal Neurons through Synaptic Plasticity. Journal of Neuroscience 35: 9946-9956.

Wilson CJ, Groves PM (1980) Fine structure and synaptic connections of the common spiny neuron of the rat neostriatum: a study employing intracellular inject of horseradish peroxidase. Journal of Comparative Neurology 194: 599-615.

Xu NL, Harnett MT, Williams SR, Huber D, O'Connor DH, Svoboda K, Magee JC (2012) Nonlinear dendritic integration of sensory and motor input during an active sensing task. Nature 492: 247-251.

Yovell Y, Abrams TW (1992) Temporal asymmetry in activation of Aplysia adenylyl cyclase by calcium and transmitter may explain temporal requirements of

conditioning. Proceedings of the National Academy of Sciences of the United States of America 89: 6526-6530.

Acknowledgments

I express my gratitude to my advisor Professor Haruo Kasai for invaluable mentorship. I thank Dr. Akiko Hayashi-Takagi, Dr. Shin Ishii, Dr. Hidetoshi Urakubo, Dr. Kozo Kaibuchi, Dr. Kenji Doya, Dr. Jeff Wickens, Dr. Taro Toyoizumi and Dr. Kiyoto Kasai for helpful discussion, Dr. Graham C.R. Ellis-Davies for CDNI-glutamate, Dr. Karl Deisseroth for the channelrhodopsin-2 plasmids, Dr. Michel Z. Lin for the Camuiα-CR and AKAR2-CR plasmids, Dr. Kazuya Iwamoto and Dr. Seiichiro Jinde for confocal microscopy, Ms. Masumi Ikeda for technical assistance and Ms. Mie Ogasawara and Mr. Kazuhito Tamura for laboratory facility.